universität
wien

DIPLOMARBEIT / DIPLOMA THESIS

Titel der Diplomarbeit / Title of the Diploma Thesis

The Sod Shock Tube Problem

Analytical vs. Numerical Solution

verfasst von / submitted by

Patrick Steyrleithner, Bakk. rer. nat. MSc

angestrebter akademischer Grad / in partial fulfillment of the requirements for the degree of

Magister der Naturwissenschaften (Mag. rer. nat.)

Wien, 2020 / Vienna, 2020

Studienkennzahl lt. Studienblatt / degree programme code as it appears on the student record sheet:	UA 190 412 406
Studienrichtung lt. Studienblatt / degree programme as it appears on the student record sheet:	Lehramtsstudium UF Physik UF Mathematik
Betreut von / Supervisor	Dr. Maria Charina, Privatdoz.

Contents

Chapter 1

Introduction

This diploma thesis deals with the comparison of the analytical and numerical solutions of the "Sod Shock Tube Problem", which is a test for the accuracy of computational fluid codes. In physics, fluid dynamics describes the flow of fluids, such as liquids and gases. It is said that a computational code works well, if it can resolve shocks and shock waves at different scales and magnitudes.

Shocks occur on many occasions in nature. Ben-Dor et al. (2000) states that the most natural shock wave is the sound produced by a lightning, i.e. the thunder, or sound made by a falling meteor that breaches the sound barrier. Another example for the generation of a natural shock wave is a volcanic explosion. A shock wave artificially produced by man is for example the cracking of a whip and an explosion of gunpowder (Ben-Dor et al., 2000), or by a strong electrical discharge (Zel'dovich and Raizer, 1966).

Despite the different origins of shock waves, either natural or man made, there have been several different definitions and descriptions of a shock wave made over time!

Ben-Dor et al. (2000) give a historical overview to shocks and their nomenclature. The authors state that in the 19th century Riemann used the term *shock compression* and *compression wave* for his illustration of the jump-like steepening of a wave front. Toepler was the first to use the term *shock wave* in the literature. Rankine used the term *abrupte disturbance*, while Hugoniot used the term *discontinuity*. Mach, on the other hand, used also the term *shock wave*, but also *Riemann wave*, *bang wave* and *explosion wave*. One can see that some expressions are still used nowadays, e.g. *shock wave* and *discontinuity*. Those two terms also appear in this thesis later on. The above selection of facts and persons is made by the author due to their relevance to the literature and to this thesis.

A more modern description by Ben-Dor et al. (2000) tries to define a shock wave from a physical point of view:

"Shock waves are mechanical waves of finite amplitudes and arise when matter is subjected to a rapid compression."

Silber et al. (2018), on the other hand, state that

"any object moving at velocities higher than the local speed of sound of the medium creates a disturbance which is called a shock wave.",

whereas Lequeux (2010) defines a shock

"as a result of violent increase of pressure, which produces supersonic motions."

Furthermore, Zel'dovich and Raizer (1966) write

"From a mathematical point of view, a discontinuity can be regarded as the limiting case of very large but finite gradients in the flow variables across a layer whose thickness tends to zero."

Lequeux (2010) moreover distinguishes between a discontinuity where a flow of matter is present, called a *shock wave*, and a discontinuity without any flow of matter, called a *contact discontinuity*.
Despite this variety of definitions, most of them involve velocity or pressure and the following compression of a fluid.
Therefore, a shock wave is typically generated when the velocity of a fluid, e.g. a gas or liquid, is faster than the local speed of sound. This can be quantified by the Mach number, which is the ratio of the fluid velocity and the local sound speed. A Mach number lower than 1 results in a sub-sonic flow, whereas a Mach number larger than 1 results in a super-sonic flow, with the occurrence of a shock wave.
Besides the different ways to define or name a shock wave, there are also different types of shock waves, depending on their environment. Lequeux (2010) distinguishes between shocks with or without a magnetic field and a multi-fluid shock. Shocks without a magnetic field can be described with the jump-shock or Rankine-Hugoniot conditions. If a magnetic field is present, the description of a shock becomes more complicated due to appearance of the Alfvén waves. A multi-fluid shock consists of a neutral or molecular component and a partly ionised gas component, which interacts with magnetic fields. If the ion density is very low, collisions are rare between these two components, and they can be considered as dynamically distinct components.
For simplicity, only "normal" shocks without a magnetic field and a single fluid are considered in this thesis.

Chapter 2 describes the basic mathematical principles which describe the motion of a fluid. This will be done in two different ways.
Firstly, for the continuous description of the fluids motion, the reader will get an overview of what kind of differential equations will be used. There the author refers to Ferziger and Peric (2002); Trangenstein (2009); Durran (2010) and Rieutord (2015). Further on, for the derivation

of the Euler equations from the basic physical principles, the author refers to Christodoulou and Miao (2012) and Rieutord (2015) for the conservation of mass, to Landau and Lifshitz (1987) and Christodoulou and Miao (2012) for the conservation of momentum and to Toro (2009) for the conservation of energy.
Secondly, for the discrete description of a fluids motion, for the use in numerical simulations, the author refers to Ferziger and Peric (2002) and Durran (2010) for the description on the discretisation and the use of the finite volume method. The description of the method by Gudonov for solving the discretised equations, follows Sod (1978); Toro (2009) and Durran (2010).
Also the author refers to Toro (2009) and Durran (2010) for the explanations on how to calculate the time step in numerical codes.
As an independent part to this diploma thesis, the author has written a computational code in Fortran90 to calculate the numerical solution of the underlying continuous problem. Important parts of this code will be included at the respective places within this thesis.

In chapter 3 the author will give an overview of occurrences of shocks on different scales of spacial magnitudes, and discuss how to study shocks.
Beginning at the smallest scale, the author refers to Silber et al. (2018) for meteors. For the application on stellar winds, the author refers to Raymond (2018), and on the interstellar medium to Lequeux (2010); Zajacek et al. (2019). At the largest scale of galaxies, the author will refer to Chung et al. (2009) and Yun et al. (2019).
For a brief explanation on how to study shocks now and then, the author will refer to Zel'dovich and Raizer (1966); Sod (1978) and Ben-Dor et al. (2000).

In chapter 4 the actual "Sod Shock Tube Problem" will be described, and the initial conditions selected according to Sod (1978). Moreover, the derivation of the analytical solution to this problem will be described. There the author refers mainly to Sod (1978) and Toro (2009).

In chapter 5 the results of the numerical solutions will be explained and compared graphically to the analytical solution, and discussed in chapter 6.

Chapter 2

Fundamental Principles

In this chapter the reader will get a mathematical background to hydrodynamics, as well as to its continuous and discrete (numerical) description. Furthermore, it will be explained how to build a hydrodynamical grid code in the discrete setting using the Euler equations and some examples how to implement the required equations with `FORTRAN` (F90).

2.1 Used Variables

Table 2.1 provides the reader with a list of frequently used variables within this diploma thesis. The units of these variables are given in the *cgs*-system, as widely used in astrophysics.

Table 2.1: Descriptions of used variables and their units.

Variable	Unit	Description
x	cm	position
t	s	time
ρ	$\mathrm{g\,cm^{-3}}$	mass density
p	$\mathrm{dyne\,cm^{-2}}$	pressure
u	$\mathrm{cm\,s^{-1}}$	velocity
e	$\mathrm{erg\,g^{-1}}$	specific internal energy
E	$\mathrm{erg\,g^{-1}}$	specific total energy
h	$\mathrm{erg\,g^{-1}}$	specific enthalpy
γ	$-$	adiabatic index
a	$\mathrm{cm\,s^{-1}}$	sound speed
V	$\mathrm{cm^3}$	volume
S	$\mathrm{cm^2}$	surface

continued on the next page

Table 2.1: continued.

Variable	Unit	Description
F	N	force
$\mathbf{v}$	$\mathrm{cm\,s^{-1}}$	velocity vector
$\mathbf{p}$	$\mathrm{dyne\,cm^{-2}}$	pressure vector
$\vec{p}$	$\mathrm{g\,cm\,s^{-1}}$	momentum vector

2.2 Continuous Description

For the continuous description the Euler method is used, which uses the Euler equations for compressible, inviscid fluids, which correspond to the Navier-Stokes equations with zero viscosity and without heat conduction (Steyrleithner, 2015). The Euler equations are a system of first order nonlinear hyperbolic partial differential equations.
Ferziger and Peric (2002) state that most methods to solve the Euler equations are of a hyperbolic form and Trangenstein (2009) says that hyperbolic equations are most commonly associated with advection.
A first-order quasi-linear hyperbolic equation is given by (Durran, 2010)

$$A(x,t,u)\,\frac{\partial u}{\partial t} + B(x,t,u)\,\frac{\partial u}{\partial x} = C(x,t,u)\,, \qquad x \in \mathbb{R},\, t > 0\,, \tag{2.1}$$

where A, B, C are real-valued functions, of space x, time t and velocity $u(x,t)$, and have continuous first derivatives. Durran (2010) further states that "the evolution of the solution is particularly simple when $C = 0$ and $B/A = c$" is some constant, where Eq. 2.1 reduces to, also given by Trangenstein (2009),

$$\frac{\partial u}{\partial t} + c\frac{\partial u}{\partial x} = 0\,, \qquad x \in \mathbb{R},\, t > 0\,. \tag{2.2}$$

The mathematical description of the state of a moving fluid is determined by the three dimensional velocity $\mathbf{v} = \mathbf{v}(\mathbf{x},t) = (u,v,w)$ and two thermodynamical quantities, such as the pressure $p = \mathbf{p}(\mathbf{x},t)$ and the mass density $\rho = \rho(\mathbf{x},t)$, where $\mathbf{x}$ is the three dimensional position $\mathbf{x} = (x,y,z)$ (Christodoulou and Miao, 2012).
The Euler equations are derived (subsections 2.2.1, 2.2.2 and 2.2.3) from the general principles of the conservation of mass, momentum and energy (Rieutord, 2015), and are given by equation 2.9, 2.17 and 2.26, respectively.

2.2.1 Mass Conservation

Considering a fixed volume V in $\mathbb{R}^3$, the mass within this volume can be described as

$$M(t) = \int_V \rho(\mathbf{x}, t)\, dV\,, \quad t > 0\,. \tag{2.3}$$

The change of mass through a volume is given by the mass flux $\rho\mathbf{v}$ crossing the volumes surface S. Therefore,

$$\frac{dM(t)}{dt} = -\int_S \rho(\mathbf{x}, t)\mathbf{v}\, d\mathbf{S}\,, \tag{2.4}$$

$$\frac{d}{dt}\int_V \rho(\mathbf{x}, t)\, dV = -\int_S \rho(\mathbf{x}, t)\mathbf{v}\, d\mathbf{S}, \tag{2.5}$$

where the negative sign describes a mass flux out of the volume through its surface. By interchanging the order of the differentiation and integration and applying the Gauss theorem (Bartsch, 2007, page 555) which states

$$\int_V \nabla\cdot\mathbf{V}\, dV = \int_S \mathbf{V}\, d\mathbf{S}\,, \quad d\mathbf{S} = \mathbf{n}\, dS\,, \tag{2.6}$$

where $\mathbf{V}$ is a vector and $\mathbf{n}$ is the normal vector to the surface. The right hand side of Eq. 2.5 transforms into a volume integral,

$$\int_V \frac{\partial\rho}{\partial t}\, dV = -\int_V \nabla\cdot(\rho\mathbf{v})\, dV \tag{2.7}$$

where $\nabla\cdot(\rho\mathbf{v})$ is the divergence $\nabla\cdot\mathbf{v} = \frac{\partial v_x}{\partial x} + \frac{\partial v_y}{\partial y} + \frac{\partial v_z}{\partial z}$. Rearranging Eq. 2.7, one gets

$$\int_V \frac{\partial\rho}{\partial t} + \nabla\cdot(\rho\mathbf{v})\, dV = 0. \tag{2.8}$$

Equation 2.8 holds for any volume V, thus, the integrand in Eq. 2.8 must vanish (Rieutord, 2015; Christodoulou and Miao, 2012), leading to

$$\frac{\partial\rho}{\partial t} + \nabla\cdot(\rho\mathbf{v}) = 0, \quad \mathbf{x}\in\mathbb{R}^3,\, t > 0. \tag{2.9}$$

Equation 2.9 is also known as the continuity equation.

2.2.2 Momentum Conservation

The conservation of momentum can be derived from the Newton's law

$$\frac{d\vec{p}}{dt} = \mathbf{F}(\mathbf{x}, t), \tag{2.10}$$

where $\vec{p} = \rho\mathbf{v}(\mathbf{x}, t)$ is the momentum and $\mathbf{F}$ the force (Christodoulou and Miao, 2012). The total force acting on the volume V can be written as the surface integral of the pressure (Landau and Lifshitz, 1987). The Eq. 2.10 reads then

$$\frac{d}{dt}\int_V \rho\mathbf{v}\, dV = -\int_S p\, d\mathbf{S}. \tag{2.11}$$

Transforming the right hand side of Eq. 2.11 into a volume integral, by applying Gauss's theorem (Eq. 2.6), and interchanging the order of the differentiation and integration, one gets

$$\int_V \frac{\partial\rho\mathbf{v}}{\partial t}\, dV = -\int_V \nabla p\, dV, \tag{2.12}$$

where ∇p is the pressure gradient $\nabla p = (\frac{\partial p}{\partial x}, \frac{\partial p}{\partial y}, \frac{\partial p}{\partial z})$. Analogously to the conservation of mass, the volume integrand vanishes, resulting in

$$\rho\frac{d\mathbf{v}}{dt} = -\nabla p\,, \quad \mathbf{x} \in \mathbb{R}^3,\, t > 0\,. \tag{2.13}$$

The equation of motion (Eq. 2.13) can be written now as the force $-\nabla p$ equal to the product of the acceleration $\frac{d\mathbf{v}}{dt}$ and the volume density ρ. Landau and Lifshitz (1987) state, that this derivative does not describe the change of the fluid velocity at a fixed point in space but the change of velocity of a moving particle within the fluid. Therefore, the change of velocity $d\mathbf{v}$ can be written as

$$d\mathbf{v} = \frac{\partial\mathbf{v}}{\partial t}dt + (d\mathbf{r}\cdot\nabla)\mathbf{v}\,, \tag{2.14}$$

where $d\mathbf{v}$ can be separated into the change of velocity at a fixed point in space during the time dt and the difference between the velocities at two points that are the distance $d\mathbf{r}$ apart. $d\mathbf{r}$ is the distance that a moving particle travelled during the time dt (Landau and Lifshitz, 1987). Equation 2.14 can be rewritten as

$$\frac{d\mathbf{v}}{dt} = \frac{\partial\mathbf{v}}{\partial t} + (\mathbf{v}\cdot\nabla)\mathbf{v}\,. \tag{2.15}$$

Equation 2.15 can be substituted into Eq. 2.13, resulting in

$$\rho \frac{\partial \mathbf{v}}{\partial t} + (\mathbf{v} \cdot \nabla)\mathbf{v} = -\nabla p\,, \tag{2.16}$$

or by bringing the pressure gradient to the left side one gets the equation of momentum conservation

$$\rho \frac{\partial \mathbf{v}}{\partial t} + (\mathbf{v} \cdot \nabla)\mathbf{v} + \nabla p = 0\,, \quad \mathbf{x} \in \mathbb{R}^3,\, t > 0. \tag{2.17}$$

2.2.3 Energy Conservation

The total energy within a given volume is given by

$$E_{tot}(t) = \int_V E(\mathbf{x}, t)\, dV\,, \quad t > 0\,, \tag{2.18}$$

where $E(\mathbf{x}, t)$ is the energy within a volume element dV of the volume V. If one considers the energy

$$E_S(t) = -\int_S p\mathbf{v}(\mathbf{x}, t)\, d\mathbf{S}\,, \quad t > 0\,, \tag{2.19}$$

at the surface of a given volume, which corresponds to the work done by the pressure p (Toro, 2009), one gets the energy flux E_S through the volumes surface. The change of the total energy E_{tot} per unit time is given by the derivative

$$\frac{dE(t)}{dt} = \frac{\partial E}{\partial t} + \mathbf{v} \cdot \nabla E\,, \quad t > 0\,, \tag{2.20}$$

which arises from the total derivative, given for a scalar valued function $\phi(\mathbf{x}, t)$, by

$$\frac{d}{dt}\phi(\mathbf{x}, t) = \frac{\partial \phi}{\partial t} + \mathbf{v} \cdot \nabla \phi\,, \tag{2.21}$$

where $\mathbf{v}$ is the fluid velocity. The left-hand side of Eq. 2.20 transforms in the integral form into

$$\frac{dE_{tot}(t)}{dt} = \int_V \frac{\partial E}{\partial t} dV + \int_S E\mathbf{v}\, d\mathbf{S}\,, \quad t > 0\,. \tag{2.22}$$

According to the preservation of energy, the energy surface flux out of the volume in Eq. 2.19 must be equal to the change of the energy within the volume and the energy flux inwards.

$$E_S = -\int_S p\mathbf{v}\, d\mathbf{S} = \int_V \frac{\partial E}{\partial t} dV + \int_S E\mathbf{v}\, d\mathbf{S}\,. \tag{2.23}$$

Equation 2.23 can be rearranged to

$$\int_V \frac{\partial E}{\partial t} dV = -\int_S \mathbf{v}(E+p)\, d\mathbf{S}\,. \tag{2.24}$$

By applying Gauss's theorem (Eq. 2.6), Eq. 2.24 transforms into

$$\int_V \frac{\partial E}{\partial t} dV = -\int_V \nabla \cdot [\mathbf{v}(E+p)]\, dV\,. \tag{2.25}$$

Analogously to the conservation of mass and momentum, the integrand vanishes and by rearranging one gets the equation of the conservation of energy

$$\frac{\partial E}{\partial t} + \nabla \cdot [\mathbf{v}(E+p)] = 0\,, \qquad \mathbf{x} \in \mathbb{R}^3,\, t > 0. \tag{2.26}$$

2.2.4 Hydrodynamic Equations

For simplicity, in the rest of this thesis only the one dimensional case (1D) will be considered. Therefore, the hydrodynamic Euler equations, given by Eq. 2.9, 2.17 and 2.26 can be written as (Toro, 2009; Steyrleithner, 2015)

$$\frac{\partial \mathbf{U}}{\partial t} + \frac{\partial \mathbf{F}(\mathbf{U})}{\partial x} = 0\,, \tag{2.27}$$

$$\mathbf{U} = \begin{pmatrix} \rho \\ \rho u \\ \rho E \end{pmatrix}\,, \qquad \mathbf{F}(\mathbf{U}) = \begin{pmatrix} \rho u \\ \rho u^2 + p \\ u(\rho E + p) \end{pmatrix}\,, \tag{2.28}$$

or, written out separately as

$$\frac{\partial \rho}{\partial t} + \frac{\partial (\rho u)}{\partial x} = 0\,, \tag{2.29}$$

$$\frac{\partial (\rho u)}{\partial t} + \frac{\partial}{\partial x}(\rho u^2 + p) = 0\,, \tag{2.30}$$

$$\frac{\partial (\rho E)}{\partial t} + \frac{\partial}{\partial x}[u(\rho E + p)] = 0\,, \qquad x \in \mathbb{R}, t > 0\,, \tag{2.31}$$

Figure 2.1: Illustration of the cell size Δx of a computational domain on the interval $[a, b]$.

with an additional initial condition

$$u(x, 0) = u_0(x)\,, \qquad x \in \mathbb{R}\,. \tag{2.32}$$

2.3 Discrete Description: weak solution

To evaluate the Euler equations 2.9, 2.17 and 2.26 numerically, their continuous forms need to be transferred into discrete counterparts, at a grid of equally spaced points on the intervals $[0, T]$ in time and $[a, b]$ in space.

To calculate the physical states of a fluid such as the density ρ, the pressure p, the velocity u and the total energy E, the computational domain in space $[a, b]$ is divided into single cells (Fig. 2.1). To get the size Δx of a single cell, e.g. $[x_{i-2}, x_{i-1}]$, the length of a computational domain is divided by the number of cells n_{cell},

$$\Delta x = \frac{b - a}{n_{cell}}\,, \tag{2.33}$$

where a is the left and b the right boundary. If one assumes a unity length, then $b - a = 1$.

The discretisation in time will be described later in subsection 2.3.3.

In fluid dynamics, many partial differential equations can be expressed as a system of conservation laws (Durran, 2010). To calculate the surface integrals of the conservation of mass, momentum and energy exactly, one needs to know the integrand of the flux everywhere on the surface. This information is not available, because only the spacial average of a state variable is know at the centre of a computational cell. Therefore the cell-face values must be approximated in terms of the central values (Ferziger and Peric, 2002). For these approximations, the *finite volume method* is used (Durran, 2010; Ferziger and Peric, 2002), where each point of the computational grid is surrounded by a small volume.

The position of the centre of a computational cell is given by

$$x_i = a + (2i - 1) \cdot \frac{\Delta x}{2}\,, \qquad i = 1, \ldots, n_{cell}\,, \tag{2.34}$$

whereas the position of the cell surfaces is given by $x_{i+\frac{1}{2}} = x_i + \frac{\Delta x}{2}$ with $i = 1, \dots n_{cell} - 1$.

Durran (2010) says that "if a function contains a discontinuity, it cannot be the solution to a partial differential equation in conventual sense, because derivatives are not defined at the discontinuity". Durran (2010) continues that "the solution is required to satisfy a family of related integral equations". According to Durran (2010), integrating the scalar form of the conservation law (Eq. 2.27) over the intervals $[x_i, x_{i+1}]$ and $[t, t + \Delta t]$, one obtains

$$\int_{x_i}^{x_{i+1}} \mathbf{U}(x, t + \Delta t) dx = \int_{x_i}^{x_{i+1}} \mathbf{U}(x, t) dx + \int_{t}^{t+\Delta t} \mathbf{F}\left(\mathbf{U}(x_i, t)\right) dt - \int_{t}^{t+\Delta t} \mathbf{F}\left(\mathbf{U}(x_{i+1}, t)\right) dt\,, \tag{2.35}$$

where t is the current time and $t + \Delta t$ is advanced time (see subsection 2.3.3). "An approximation to the scalar conservation law (Eq. 2.27) is in conservation form if" (Durran, 2010)

$$\frac{\mathbf{U}_i^{n+1} - \mathbf{U}_i^n}{\Delta t} + \frac{\mathbf{F}_{i+\frac{1}{2}} - \mathbf{F}_{i-\frac{1}{2}}}{\Delta x} = 0\,, \tag{2.36}$$

where $\mathbf{F}_{i\pm\frac{1}{2}}$ are numerical approximations of the fluxes $\mathbf{F}(\mathbf{U}(x_{i\pm\frac{1}{2}}, t))$.
By using the finite-volume method, Durran (2010) says, that if $\mathbf{U}_i^n$ approximates the spacial average of a state variable $\mathbf{U}$ over a grid cell x_i, then the approximation at a time t^n is given by

$$\mathbf{U}_i^n \approx \frac{1}{\Delta x} \int_{x_{i-\frac{1}{2}}}^{x_{i+\frac{1}{2}}} \mathbf{U}(x, t^n)\, dx\,, \quad n \in \mathbb{N}\,. \tag{2.37}$$

The flux $\mathbf{F}_{i\pm\frac{1}{2}}$ is the approximation of the time-averaged flux through the interface $x_{i\pm\frac{1}{2}}$ between cells with centres x_i and $x_{i\pm1}$, given by

$$\mathbf{F}_{i\pm\frac{1}{2}} \approx \frac{1}{\Delta t} \int_{t^n}^{t^{n+1}} \mathbf{F}\big(\mathbf{U}(x_{i\pm\frac{1}{2}}, t)\big)\, dt\,. \tag{2.38}$$

Averaging the conservation law (Eq. 2.27) over an i-th cell and integrating over a single time step, where $t^{n+1} = t + \Delta t$, the integral form of Eq. 2.35 can then be written as

$$\int_{x_{i-\frac{1}{2}}}^{x_{i+\frac{1}{2}}} \mathbf{U}(x, t^{n+1})\, dx = \int_{x_{i-\frac{1}{2}}}^{x_{i+\frac{1}{2}}} \mathbf{U}(x, t^n)\, dx - \left(\int_{t^n}^{t^{n+1}} \mathbf{F}\big(\mathbf{U}(x_{i+\frac{1}{2}}, t)\big)\, dt - \int_{t^n}^{t^{n+1}} \mathbf{F}\big(\mathbf{U}(x_{i-\frac{1}{2}}, t)\big)\, dt \right)\,. \tag{2.39}$$

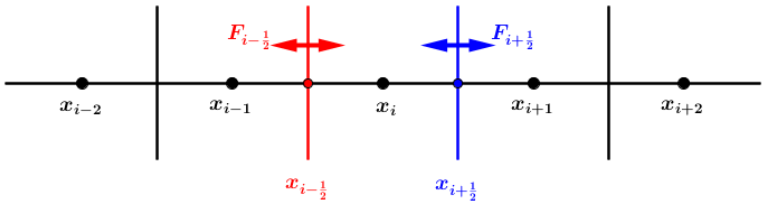

Figure 2.2: The flux vector $\mathbf{F}_{i-\frac{1}{2}}$ denotes to the flux through the cell interface $x_{i-\frac{1}{2}}$ between the cells x_{i-1} and x_i (red), and the flux vector $\mathbf{F}_{i+\frac{1}{2}}$ denotes to the flux through the cell interface $x_{i+\frac{1}{2}}$ between the cells x_i and x_{i+1} (blue).

By using the approximations 2.37 and 2.38, the above expression can be written as

$$\mathbf{U}_i^{n+1}\Delta x = \mathbf{U}_i^n \Delta x - \Delta t \left(\mathbf{F}_{i+\frac{1}{2}} - \mathbf{F}_{i-\frac{1}{2}}\right) . \tag{2.40}$$

By dividing Eq. 2.40 with the cell size Δx, the scalar form of the conservation law (Eq. 2.27) can be approximated by

$$\begin{aligned} \mathbf{U}_i^{n+1} &= \mathbf{U}_i^n - \frac{\Delta t}{\Delta x}\left(\mathbf{F}_{i+\frac{1}{2}} - \mathbf{F}_{i-\frac{1}{2}}\right) , \\ i &= 1, \ldots, n_{cell} , \\ n &\in \mathbb{N}_0 . \end{aligned} \tag{2.41}$$

2.3.1 Hydrodynamic Solver

To further on describe the discretisation of the Euler equations (2.29 − 2.30) with the approximation of Eq. 2.41, Gudonov's first-order *upwind method* (Toro, 2009; Durran, 2010) is used. In Eq. 2.41, $\mathbf{U}_i^n$ is the state vector at the x_i-th cell at time t^n, $\mathbf{U}_i^{n+1}$ is the state vector at the new time t^{n+1}. $\mathbf{F}$ is the flux vector, Δt is the time step and Δx the size of a computational cell. The flux vector $\mathbf{F}_{i-\frac{1}{2}}$ denotes to the flux through the cell interface between the cells x_{i-1} and x_i, and the flux vector $\mathbf{F}_{i+\frac{1}{2}}$ through the interface between the cells x_i and x_{i+1} (see Fig. 2.2). The value $\mathbf{U}_i^n$ at time t^n will then be updated to the new value $\mathbf{U}_i^{n+1}$ at time t^{n+1}.
For the data at the time t^n one assumes that they are a pair of constant states separated by a discontinuity, the cell interface (Toro, 2009). Each cell represents then two Riemann problems, one for each interface, left and right.
A Riemann problem is an initial value problem given by a partial differential equation, e.g. Eq. 2.27, with a set of initial conditions, e.g. Eq. 4.1. For this initial value problem, the initial conditions consist of piecewise constant initial data that has a discontinuity.
There are two possible values at each interface which can be chosen from. For example at the interface $x_{i-\frac{1}{2}}$, the flux can be positive or negative, moving to the right or left, respectively. Figure 2.3 illustrates the two possibilities.

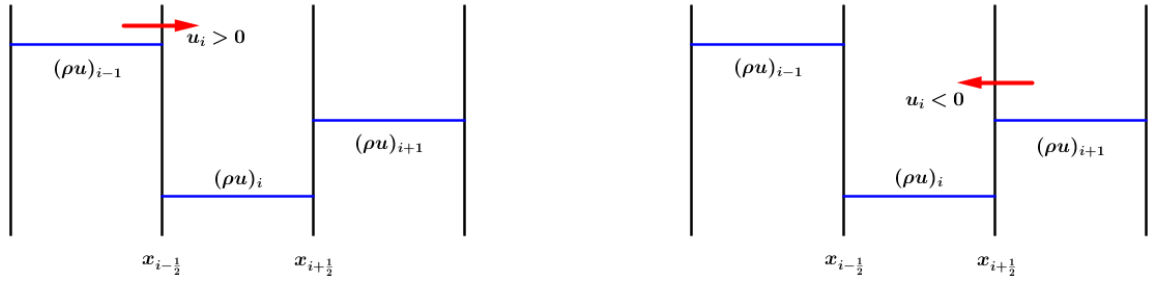

Figure 2.3: The blue horizontal lines indicate the different values of the momentum and the red arrows indicate the direction of the movement. Left: The centred velocity u_i of the central cell is positive, therefor the fluid moves to the right through the interface $x_{i-\frac{1}{2}}$ between the cells x_{i-1} and x_i; Right: The centred velocity u_i of the central cell is negative, therefor the fluid moves to the left through the interface $x_{i+\frac{1}{2}}$ between the cells x_i and x_{i+1}.

To advect the fluid properly, one must chose the correct flux based on the fluids velocity. Therefore Sod (1978) proposed the following method depending on the velocity of the fluid in the central cell that one is solving for.

$$\mathbf{F}_{i-\frac{1}{2}} = \begin{cases} \mathbf{F}_i & \text{if } u_i > 0 \\ \mathbf{F}_{i-1} & \text{if } u_i < 0 \end{cases} \tag{2.42}$$

$$\mathbf{F}_{i+\frac{1}{2}} = \begin{cases} \mathbf{F}_{i+1} & \text{if } u_i > 0 \\ \mathbf{F}_i & \text{if } u_i < 0 \end{cases} \tag{2.43}$$

The advection of the new values of the density, pressure and energy for a single cell are then given by

$$\rho_i^{n+1} = \rho_i^n + \frac{\Delta t}{\Delta x}\left\{(\rho u)_{i-\frac{1}{2}} - (\rho u)_{i+\frac{1}{2}}\right\} \tag{2.44}$$

$$(\rho u)_i^{n+1} = (\rho u)_i^n + \frac{\Delta t}{\Delta x}\left\{\left(\rho u^2\right)_{i-\frac{1}{2}} - \left(\rho u^2\right)_{i+\frac{1}{2}}\right\} - \Delta t\, \nabla p_i \tag{2.45}$$

$$(\rho E)_i^{n+1} = (\rho E)_i^n + \frac{\Delta t}{\Delta x}\left\{(u\rho E)_{i-\frac{1}{2}} - (u\rho E)_{i+\frac{1}{2}}\right\} - \frac{\Delta t}{2\Delta x}\left\{(up)_{i+1} - (up)_{i-1}\right\}. \tag{2.46}$$

The pressure gradient is given by

$$\nabla p_i = \frac{p_{i+1} - p_{i-1}}{2\Delta x}\,, \tag{2.47}$$

where the pressure will be expressed through the components of the state vector 2.28

$$p = (\gamma - 1)\,\rho \left(E - \frac{1}{2}u^2\right) \tag{2.48}$$

$$= (\gamma - 1) \left[(\rho E) - \frac{1}{2}\left(\rho u^2\right)\right] \tag{2.49}$$

$$= (\gamma - 1) \left[(\rho E) - \frac{1}{2}\frac{(\rho u)^2}{\rho}\right]\,. \tag{2.50}$$

Code 2.1: Advection of the density, momentum and energy of a fluid.

```
! checking in which direction the fluid moves
  IF ( U(2,i) .GE. 0. ) THEN
    a = 1; b = 0  ! if the fluid moves to the right
  ELSE
    a = 0; b = -1 ! if the fluid moves to the left
  END IF

! ---- density ---- !
  ! calculating the fluxes
  fluxLeft  = U(2,i-1*a)
  fluxRight = U(2,i-1*b)
  ! calculating the new values of the density
  U_new(1,i) = U(1,i) + (dt / dx) * ( fluxLeft - fluxRight )

! ---- momentum ---- !
  ! calculating the pressure gradient
  gradP(i) = ( pres(i) + pres(i-1) ) / ( 2. * dx)
  ! calculating the fluxes
  fluxLeft  = U(2,i-1*a)**2 / U(1,i-1*a)
  fluxRight = U(2,i-1*b)**2 / U(1,i-1*b)
  ! calculating the new values for the momentum
  U_new(2,i) = U(2,i) + (dt / dx) * ( fluxLeft - fluxRight ) - dt * gradP(i)

! ---- energy ---- !
  ! calculating the fuxes
  fluxLeft  = U(2,i-1*a) * U(3,i-1*a) / U(1,i-1*a)
  fluxRight = U(2,i-1*b) * U(3,i-1*b) / U(1,i-1*b)
  ! calculating the new values for the momentum
  U_new(3,i) = U(3,i) + (dt / dx) * ( fluxLeft - fluxRight )
  ! adding the pressure component
```

```
31   fluxLeft  = U(2,i+1) * pres(i+1) / U(1,i+1)
32   fluxRight = U(2,i-1) * pres(i-1) / U(1,i-1)
33   ! updating the new values with the pressure component
34   U_new(3,i) = U_new(3,i) - ( dt / (2. * dx) ) * ( fluxLeft - fluxRight )
```

2.3.2 The Courant-Friedrichs-Lewy Condition

The Courant number or CFL coefficient (Durran, 2010; Toro, 2009) is given by

$$C_{cfl} = c\frac{\Delta t}{\Delta x} \tag{2.51}$$

$$= \frac{c}{\Delta x/\Delta t} \tag{2.52}$$

where c is the speed of a wave within the fluid, Δt is the time step and Δx is the size of a computational cell. The Courant number C_{cfl} gives the ratio between the fluid speed and the effective grid speed, the speed the fluid would need to travel at to cross the cell in a single time step. The current scheme to advect the fluid would be unstable if $C_{cfl} > 1$, which means that the fluid would travel across more than one cell in a single time step. With this and the fact that the size of a computation cell Δx and the time step Δt are positive, the CFL condition can be written as

$$0 \leq C_{cfl} \leq 1\,. \tag{2.53}$$

2.3.3 Time Step

To compute the advection time step, the CFL condition is used to guarantee that no wave present in the fluid travels more than the distance Δx in the time Δt (Durran, 2010; Toro, 2009). The time step is then given by

$$\Delta t = C_{cfl}\,\frac{\Delta x}{S^n_{max}}\,, \tag{2.54}$$

where C_{cfl} is the Courant number in 2.53 and S^n_{max} is the largest speed of wave present in the entire computational domain. To ensure that $\Delta t > 0$, the CFL coefficient is chosen to be larger than zero. The estimate of the largest wave speed is given by (Durran, 2010)

$$S^n_{max} = \max\left\{|u^n_i| + a^n_i\right\}\,, \tag{2.55}$$

where u^n_i is the velocity of the fluid and a^n_i the sound speed at time t^n. Durran (2010) states that Eq. 2.55 may underestimate S^n_{max}, e.g. in a shock tube, where initial velocity is zero and only the sound speed is taken into account. This underestimation will lead to a time step that

is too large, resulting in instabilities. This can be prevented by adjusting the CFL coefficient. The sound speed a in Eq. 2.55 is given by

$$a = \sqrt{\gamma \frac{p}{\rho}}, \tag{2.56}$$

where γ is the adiabatic index, ρ the density and p the pressure of the fluid. The pressure p will be calculated by Eq. 2.50 and the velocity of a fluid will then be expressed as followed.

$$u = \frac{(\rho u)}{\rho} \tag{2.57}$$

The following code 2.2 is an example how to calculate the time step Δt numerically according to Eq. 2.54 and 2.55. `U` is the state vector in Eq. 2.27 and 2.28, `gamma` is the adiabatic index γ, `dx` the size of a cell and `cfl` the CFL coefficient.

Code 2.2: Calculation of the time step Δt (`dt`).

```
1 ! calculating the pressure 'pres', the sound speed 'sound' and the fluid velocity 'velx'
2 ! in each cell
3 DO i = 1, nCell
4   pres(i)  = (gamma - 1) * ( U(3,i) - 0.5 * U(2,i)**2 / U(1,i) )
5   sound(i) = SQRT( gamma * pres(i) / U(1,i) )
6   velx(i)  = U(2,i) / U(1,i)
7 END DO
8
9 ! calculating the time step 'dt'
10 dt = cfl * dx / MAXVAL( ABS(velx(:)) + sound(:) )
```

Chapter 3

Description of Physical Phenomena

In the following subsections, the applications and study of shocks will be presented. For the application of shocks, a short historical background will be given and the use in astrophysical phenomena. Table 3.1 provides some used abbreviations in astrophysics.

Table 3.1: Astrophysical abbreviations and their descriptions.

Abbreviations	Term	Description
AGN	active galactic nucleus	compact central region of a galaxy that emits large amounts of radiation
ICM	intracluster medium	the medium within a galaxy cluster, typically hot gas
ISM	interstellar medium	medium between stars
SN	supernova	explosion of a star
SNR	supernova remnant	a structure of expanding material after the explosion of a star

3.1 Shock Applications

The scientific interest in shock waves arises around World War `I` and `II`, where new disciplines in physics arises, such as hypersonic aerodynamics, cosmic gas dynamics, reentry, detonations and nuclear explosions, and others (Ben-Dor et al., 2000).
Although Ben-Dor et al. (2000) state that shock waves have been observed in all four states of matter (solids, liquids, gases and plasma), only applications of shock waves to gases are mentioned in this thesis.

A quite interesting application of shocks can be applied in astrophysics at different scales. From a shock wave of a meteor moving through a planets atmosphere (Silber et al., 2018), e.g. the earth, to shock waves in a star and its corona and vicinity (Raymond, 2018), as well as stellar winds. Shock waves generated in the interstellar medium (ISM) due to stars moving with a high velocity (Zajacek et al., 2019) or supernovae (SNe), the explosion of a star. From shock waves produced by a galactic wind or active galactic nuclei (AGN), to shock waves in the intracluster medium (ICM) produced by an infalling galaxy or the collision of two galaxy clusters (Chung et al., 2009).
These astrophysical applications shall be explained briefly.

Meteor: A meteor is a blunt body, consisting of rocks and metals, generates a shock wave when it is moving through a gas, typically an atmosphere of a planet. Meteors, falling onto the earth, have typically velocities of around $20 - 70\,\mathrm{km\,s^{-1}}$ (Silber et al., 2018), while the speed of sound of air is about $0.343\,\mathrm{km\,s^{-1}}$. Therefore, a meteor moves with a supersonic velocity through the earths atmosphere, creating a shock wave, a so called *bow shock* in front of it (Silber et al., 2018).
While the results of an impact of a meteor are visible, as impact craters, on many planets and moons in our solar system, the direct observation a falling meteor through the earths atmosphere is sparse. But thanks to many security cameras and car cameras, the sitings of meteors is rising since a few years. The most famous Chelyabinsk meteor entered the earths atmosphere over Russia in 2013 and damaged buildings due to its air burst 30 km above Chelyabinsk (Wikipedia contributors, 2019).

Stellar Winds: A stellar or solar wind consists of charged particles, which are released from the stars upper atmosphere. Most shocks in astrophysics are collisionless, because of the magnetic fields and the interaction with charged particles (Raymond, 2018), such as protons, electrons and Helium-cores. In a close vicinity to a star, a shock can produce cosmic rays by acceleration of charged particles. Raymond (2018) states that these shocks can be produced by coronal mass ejections of a star, and can therefore affect satellites and astronauts. This is an example where "cosmic" shocks can directly affect human kind and their technology.
These stellar winds expand into the undisturbed ISM and creates then a shock wave.

ISM: During the lifetime of a star it will loose mass by stellar winds, which happens continuously over time. A star with a mass $M_* > 8\,M_\odot$ will explode at the end of its lifetime as a type II supernova, where a significant amount of its mass will be ejected into the ISM, resulting in a supernova remnant (SNR). According to Lequeux (2010), the evolution a SNR can be distinguished into three phases. Starting with the free expansion phase, which ends

when the mass of the swept up matter equals the ejected mass. Followed by the adiabatic expansion phase, also called the Sedov-Taylor phase, where the shocked gas has a such high temperature that the SNR is pressure driven. The evolution of a SNR ends with the isothermal phase due to the energy loss by radiation, where the shell dispersed by reaching about the same velocity as the ISM.
A star also produces a shock wave, during its lifetime, when it is moving through the ISM, e.g. near to the galactic centre (Zajacek et al., 2019). The created bow shock can be used to determine the motion of the star around the galactic centre by analysing the symmetry axis of the bow shock.

Galaxies: Shock waves can also be observed at a larger, galactic scale. Galaxies with active star formation experience a galactic wind or galaxies with AGN often experience a bipolar jet, resulting in a shock wave in the galaxies hot halo gas. Moreover, galaxies themselves can produce a shock wave, when they fall into a galaxy cluster and move through the hot ICM. These bow shocks can be sometimes observed in the surface density of the ICM. This phenomena can also be shown in simulations of infalling galaxies (Yun et al., 2019).
Even galaxy clusters can produce shock waves, when two of them merge together. Chung et al. (2009) show that the Bullet cluster, two merging galaxy clusters of unequal mass, experience a shock wave driven by the subcluster and propagating through the hot ICM of the main cluster.

3.2 Studying Shocks

To study shocks, one needs to produce a shock wave, which then can be studied. At first this was not easy, but in the late 19th century this became easier with a strong electrical discharge. In science one has to execute the same experiment over and over again under the same conditions. To apply this to shocks, one can use the shock tube.
The Shock Tube was invented by Paul Vieille, which is the most important measuring and testing device of gas dynamics (Ben-Dor et al., 2000). He tried to demonstrate that shock waves generated by explosions propagate analogously to a shock wave generated by a bursting diaphragm.
Such a shock tube usually has a circular or rectangular cross section and is separated by a thin diaphragm in two parts, a low and high pressure chamber (Zel'dovich and Raizer, 1966).

Nowadays fluid dynamics can be studied by numerical simulations. To ensure that a code works well, it has to be assured that it can capture and resolve shocks properly. Sod (1978) compared the performance of different numerical codes by using the numerical version of the shock tube and compare the results to the well known analytical solution. Only by this,

one can assure that the results of a numerical simulation of e.g. a supernova are physically correct.

Chapter 4

The Sod Shock Tube Problem

4.1 Initial Conditions

The "Sod Shock Tube Problem" (Sod, 1978) consists of a fluid with two different states as initial conditions, which are separated by a diaphragm at position $d = \frac{b-a}{2}$ [cm] within the interval $[a, b]$. The initial conditions are given by

$$\begin{pmatrix} \rho \\ p \\ u \end{pmatrix}(x,0) = \begin{pmatrix} 1.0 \\ 1.0 \\ 0.0 \end{pmatrix} \quad x \in [a,d) \ , \qquad \begin{pmatrix} \rho \\ p \\ u \end{pmatrix}(x,0) = \begin{pmatrix} 0.125 \\ 0.1 \\ 0.0 \end{pmatrix} \quad x \in [d,b] \tag{4.1}$$

where ρ, p and u are the density, pressure and velocity, respectively, as listed in table 2.1.

4.2 Analytical Solution

At time $t > 0$, the diaphragm is broken. Considering the situation that no wave has reached the left or right boundary. The time dependant variables $xhd(t)$ and $xft(t)$ represent the head and tail of the rarefaction wave. The variable $xcd(t)$ is the contact discontinuity, the position that an element of the fluid initially at d has reached by time $t > 0$. The variable $xsh(t)$ is the position of the shock wave, at which all the quantities (e.g. ρ and p) are discontinuous (Sod, 1978).
Figure 4.1 shows the position of the head $xhd(t)$ and foot $xft(t)$ of the rarefaction wave, the contact discontinuity $xcd(t)$ and the shock wave $xsh(t)$ as a function of time. One can see, that the rarefaction wave (dotted lines enclosed by $xhd(t)$ and $xft(t)$ in Fig. 4.1) is moving to the left, while the contact discontinuity and the shock wave are moving to the right.
As shown in Fig. 4.1, one can divide computational domain into five regions, separated by the head and tail of the rarefaction wave, the contact discontinuity and the shock wave. To

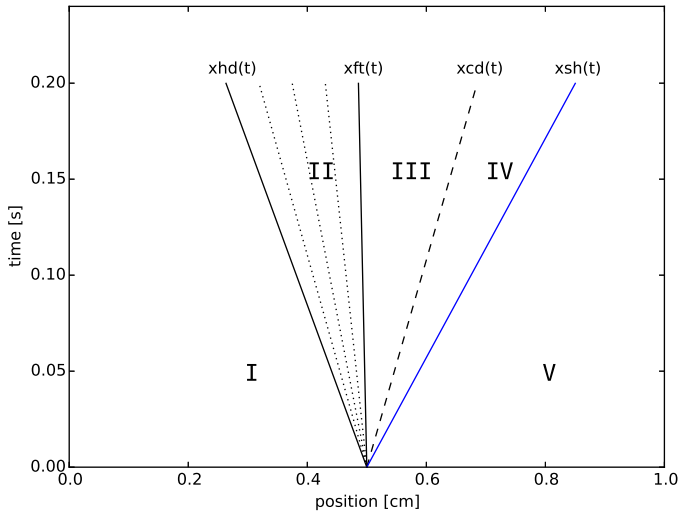

Figure 4.1: Analytic solution of the position of the head $xhd(t)$ and foot $xft(t)$ of the rarefaction wave, the contact discontinuity $xcd(t)$ and the shock wave $xsh(t)$ as a function of time for the Sod shock tube. The dotted lines represent the rarefaction wave. The computational domain is chosen to be the interval $[a, b] = [0, 1]$, and the diaphragm is initially positioned at $d = 0.5\,\text{cm}$.

derive the analytical solution it is prudent to derive the individual analytical solutions for each region. Furthermore, those shall be described in dependence of the initial conditions, which are represented by region `I` and `V`.

4.2.1 Region `I` and `V`

The solution for the states in region `I` and `V` are the initial states left and right, respectively, of the diaphragm at the time $t = 0$.

Solution for Region `I`:

$$\begin{pmatrix} \rho \\ p \\ u \end{pmatrix}(x,t) = \begin{pmatrix} 1.0 \\ 1.0 \\ 0.0 \end{pmatrix} \qquad x \in [0, xhd(t)],\ t > 0 \tag{4.2}$$

Solution for Region `V`:

$$\begin{pmatrix} \rho \\ p \\ u \end{pmatrix}(x,t) = \begin{pmatrix} 0.125 \\ 0.1 \\ 0.0 \end{pmatrix} \qquad x \in [xsh(t), 1],\ t > 0 \tag{4.3}$$

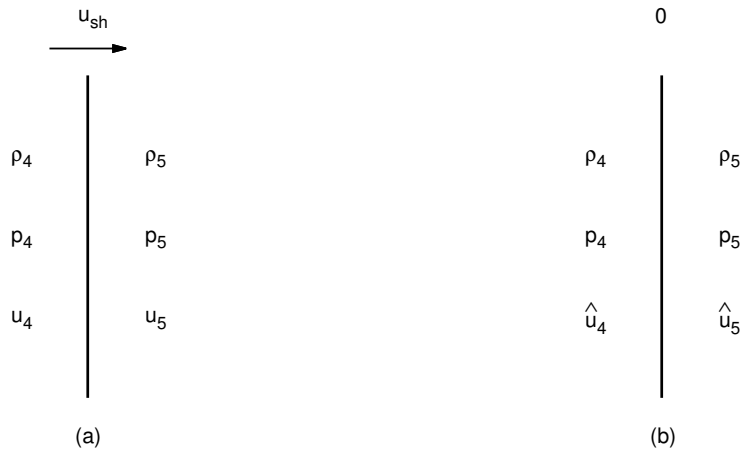

Figure 4.2: (a) shock wave in a stationary reference system (a) with the velocity of u_{sh}; (b) reference system moves with the velocity u_{sh} so that the shock front moves with zero velocity.

4.2.2 The Shock Wave

Assuming that the shock wave is moving to the right side, (ρ_5, u_5, p_5) denote the quantities ahead of the shock front and (ρ_4, u_4, p_4) behind the shock front (see Fig. 4.2). To calculate the speed of the shock wave u_{sh}, one is moving with the shock. Therefore, the new relative velocities are

$$\hat{u}_4 = u_4 - u_{sh} \tag{4.4}$$

$$\hat{u}_5 = u_5 - u_{sh}\,. \tag{4.5}$$

The Rankine-Hugoniot conditions or jump-shock conditions (Lequeux, 2010) describe a relation between the states ahead and behind the shock. Normally the the quantities ahead of the shock are indicated with the index 1 and those behind the shock with the index 2. In this case the author choses to use the indices denoting the different regions of the solution of the Sod Shock Tube Problem. Therefore, the quantities ahead of the shock have the index 5 and those behind the shock the index 4.

$$\rho_4\,\hat{u}_4 = \rho_5\,\hat{u}_5 \tag{4.6}$$

$$\rho_4\,\hat{u}_4^2 + p_4 = \rho_5\,\hat{u}_5^2 + p_5 \tag{4.7}$$

$$\hat{u}_4\left(\hat{E}_4 + p_4\right) = \hat{u}_5\left(\hat{E}_5 + p_5\right) \tag{4.8}$$

Introducing the total energy

$$E = \rho \left(\frac{1}{2} u^2 + e \right) \tag{4.9}$$

and substituting into Eq. 4.8,

$$u\ (E + p) = u\ \left[\rho \left(\frac{1}{2} u^2 + e \right) + p \right] \tag{4.10}$$

$$= u\, \rho\ \left[\frac{1}{2} u^2 + e + \frac{p}{\rho} \right] , \tag{4.11}$$

resulting in

$$\hat{u}_4\, \rho_4\ \left[\frac{1}{2} \hat{u}_4^2 + e_4 + \frac{p_4}{\rho_4} \right] = \hat{u}_5\, \rho_5\ \left[\frac{1}{2} \hat{u}_5^2 + e_5 + \frac{p_5}{\rho_5} \right] \tag{4.12}$$

Substituting the specific enthalpy

$$h = e + \frac{p}{\rho} \tag{4.13}$$

into Eq. 4.12 and using Eq. 4.6 gives

$$\frac{1}{2} \hat{u}_4^2 + h_4 = \frac{1}{2} \hat{u}_5^2 + h_5 \,. \tag{4.14}$$

Rearranging Eq. 4.6 gives

$$\hat{u}_5 = \frac{\rho_4\, \hat{u}_4}{\rho_5} \tag{4.15}$$

and rearranging Eq. 4.7 gives

$$\rho_4\, \hat{u}_4^2 = \rho_5\, \hat{u}_5^2 + p_5 - p_4 \tag{4.16}$$

$$= (\rho_5\, \hat{u}_5)\, \hat{u}_5 + p_5 - p_4 \quad | \text{ Eq. 4.15} \tag{4.17}$$

$$= (\rho_5\, \hat{u}_5) \frac{\rho_4\, \hat{u}_4}{\rho_5} + p_5 - p_4 \tag{4.18}$$

Using Eq. 4.6

$$\rho_4\, \hat{u}_4^2 = (\rho_4\, \hat{u}_4) \frac{\rho_4\, \hat{u}_4}{\rho_5} + p_5 - p_4 \tag{4.19}$$

$$= \frac{\rho_4^2\, \hat{u}_4^2}{\rho_5} + p_5 - p_4 \tag{4.20}$$

Bringing all terms with $\hat{u}_4^2$ on the left side gives

$$\rho_4 \hat{u}_4^2 - \frac{\rho_4^2 \hat{u}_4^2}{\rho_5} = p_5 - p_4 \tag{4.21}$$

$$\hat{u}_4^2 \left[\rho_4 - \frac{\rho_4^2 \hat{u}_4^2}{\rho_5} \right] = p_5 - p_4 \tag{4.22}$$

$$\hat{u}_4^2 \left[\rho_4 - \frac{\rho_4^2}{\rho_5} \right] = p_5 - p_4 \tag{4.23}$$

$$\hat{u}_4^2 \left[\frac{\rho_4 \rho_5 - \rho_4^2}{\rho_5} \right] = p_5 - p_4 \tag{4.24}$$

$$\hat{u}_4^2 \left[\frac{\rho_4}{\rho_5} \frac{\rho_5 - \rho_4}{\rho_5} \right] = p_5 - p_4 \tag{4.25}$$

$$\tag{4.26}$$

Isolating the velocity $\hat{u}_4^2$ on the left side gives

$$\hat{u}_4^2 = \left(\frac{\rho_5}{\rho_4} \right) \left(\frac{p_5 - p_4}{\rho_5 - \rho_4} \right) . \tag{4.27}$$

The same can be done for the velocity $\hat{u}_5^2$

$$\hat{u}_5^2 = \left(\frac{\rho_4}{\rho_5} \right) \left(\frac{p_5 - p_4}{\rho_5 - \rho_4} \right) . \tag{4.28}$$

Rearranging Eq. 4.14 yields

$$h_4 - h_5 = \frac{1}{2} \left[\hat{u}_5^2 - \hat{u}_4^2 \right] \tag{4.29}$$

Substituting the velocities Eq. 4.27 and 4.28, bringing to the same denominator and rearranging yields in

$$h_4 - h_5 = \frac{1}{2} \frac{(p_5 - p_4) \cancel{(\rho_5 - \rho_4)} (\rho_4^2 - \rho_5^2)}{\rho_4 \rho_5 (\rho_5 - \rho_4)^{\cancel{2}}} , \tag{4.30}$$

and using a binomial expansion gives

$$h_4 - h_5 = \frac{1}{2} (p_5 - p_4) \frac{\rho_4 + \rho_5}{\rho_4 \rho_5} . \tag{4.31}$$

Re-substituting the specific enthalpy, Eq. 4.13, to get an expression for the specific energy e gives after rearranging and bringing to the same denominator:

$$e_4 - e_5 = \frac{1}{2}\frac{(p_5 - p_4)\,(\rho_4 + \rho_5)}{\rho_4\,\rho_5} - \frac{p_4\,\rho_5 + p_5\,\rho_4}{\rho_4\,\rho_5} \tag{4.32}$$

$$= \frac{1}{2}(p_5 + p_4)\frac{\rho_4 - \rho_5}{\rho_4\,\rho_5}\,. \tag{4.33}$$

By substituting the specific energy

$$e = \frac{p}{(\gamma - 1)\,\rho}\,, \tag{4.34}$$

where γ is the ratio of specific heats, one gets an expression for the ratio of the densities behind and ahead of the shock front, dependent of the ratio of the pressure behind and ahead of the shock front and the ratio of specific heats.

$$\frac{p_4}{(\gamma-1)\rho_4} - \frac{p_5}{(\gamma-1)\rho_5} = \frac{1}{2}(p_5 + p_4)\frac{\rho_4 - \rho_5}{\rho_4\,\rho_5} \tag{4.35}$$

Bringing the left side to the same denominator and multiplying out the nominator on the right side gives

$$\frac{\cancel{(\gamma-1)}\,p_4\,\rho_5 + \cancel{(\gamma-1)}\,p_5\,\rho_4}{(\gamma-1)^{\cancel{2}}\,\cancel{\rho_4\,\rho_5}} = \frac{1}{2}\frac{p_4\,\rho_4 - p_4\,\rho_5 + p_5\,\rho_4 - p_5\,\rho_5}{\cancel{\rho_4\,\rho_5}}\,. \tag{4.36}$$

Multiplying with $(\gamma - 1)$ and dividing both sides with $(p_5\,\rho_5)$ gives

$$\frac{p_4}{p_5} - \frac{\rho_4}{\rho_5} = \frac{\gamma - 1}{2}\left[\frac{p_4}{p_5}\frac{\rho_4}{\rho_5} - \frac{p_4}{p_5} + \frac{\rho_4}{\rho_5} - 1\right]\,. \tag{4.37}$$

Isolating all terms with the ratio of densities on the left side.

$$-\frac{\rho_4}{\rho_5} - \frac{\gamma-1}{2}\frac{p_4}{p_5}\frac{\rho_4}{\rho_5} - \frac{\gamma-1}{2}\frac{\rho_4}{\rho_5} = -\frac{p_4}{p_5} - \frac{\gamma-1}{2}\frac{p_4}{p_5} - \frac{\gamma-1}{2} \tag{4.38}$$

$$\frac{\rho_4}{\rho_5}\left[-1 - \frac{\gamma-1}{2}\left(\frac{p_4}{p_5} + 1\right)\right] = \frac{p_4}{p_5}\left[-1 - \frac{\gamma-1}{2}\right] - \frac{\gamma-1}{2} \tag{4.39}$$

Isolating the ratio of densities behind and ahead of the shock front on the left side.

$$\frac{\rho_4}{\rho_5} = \frac{\frac{p_4}{p_5}\left[-1 - \frac{\gamma-1}{2}\right] - \frac{\gamma-1}{2}}{-1 - \frac{\gamma-1}{2}\left(\frac{p_4}{p_5} + 1\right)} \tag{4.40}$$

Using the algebraic manipulation

$$-1-\frac{\gamma-1}{2}=\frac{-2-\gamma+1}{2}=-\frac{\gamma+1}{2} \tag{4.41}$$

gives

$$\frac{\rho_4}{\rho_5}=\frac{\frac{p_4}{p_5}\left(-\frac{\gamma+1}{2}\right)-\frac{\gamma-1}{2}}{-1-\frac{\gamma-1}{2}\left(\frac{p_4}{p_5}+1\right)} \tag{4.42}$$

$$=-\frac{\frac{p_4}{p_5}\frac{\gamma+1}{2}+\frac{\gamma-1}{2}}{-1-\frac{\gamma-1}{2}\left(\frac{p_4}{p_5}+1\right)} \tag{4.43}$$

$$=\frac{\frac{p_4}{p_5}\frac{\gamma+1}{2}+\frac{\gamma-1}{2}}{1+\frac{\gamma-1}{2}\left(\frac{p_4}{p_5}+1\right)} \tag{4.44}$$

Dividing nominator and denominator with $\frac{\gamma-1}{2}$ gives

$$\frac{\rho_4}{\rho_5}=\frac{\frac{p_4}{p_5}\frac{\gamma+1}{\gamma-1}+1}{\frac{2}{\gamma-1}+\frac{p_4}{p_5}+1}. \tag{4.45}$$

By using the algebraic manipulation

$$\frac{2}{\gamma-1}+1=\frac{2+\gamma-1}{\gamma-1}=\frac{\gamma+1}{\gamma-1} \tag{4.46}$$

gives

$$\frac{\rho_4}{\rho_5}=\frac{\frac{p_4}{p_5}\frac{\gamma+1}{\gamma-1}+1}{\frac{\gamma+1}{\gamma-1}+\frac{p_4}{p_5}}, \tag{4.47}$$

which gives the same results as the equation by Toro (2009)

$$\frac{\rho_4}{\rho_5}=\frac{\frac{p_4}{p_5}+\frac{\gamma-1}{\gamma+1}}{\frac{\gamma-1}{\gamma+1}\frac{p_4}{p_5}+1}. \tag{4.48}$$

By introducing the Mach number

$$M_5=\frac{u_5}{a_5} \tag{4.49}$$

$$M_{sh}=\frac{u_{sh}}{a_5} \tag{4.50}$$

one can write the ratio of the density and pressure, respectively, behind and ahead of the shock front (Toro, 2009) as

$$\frac{\rho_4}{\rho_5} = \frac{(\gamma+1)\,(M_5 - M_{sh})^2}{(\gamma-1)\,(M_5 - M_{sh})^2 + 2} \tag{4.51}$$

$$\frac{p_4}{p_5} = \frac{2\gamma\,(M_5 - M_{sh})^2 - (\gamma-1)}{(\gamma+1)}\,. \tag{4.52}$$

Re-arranging the pressure ratio and re-substituting the Mach number yields to the speed of the shock wave.

$$u_{sh} = u_5 + a_5\sqrt{\frac{\gamma+1}{2\gamma}\frac{p_4}{p_5} + \frac{\gamma-1}{2\gamma}} \tag{4.53}$$

Position of the shock front:
The position of the shock front is given by

$$xsh(t) = d + u_{sh}\,t\,, \qquad t > 0\,. \tag{4.54}$$

4.2.3 Region `II`

Region `II` is bound by the head $xhd(t)$ and foot $xft(t)$ of the rarefaction wave. If one considers a ray from the point (d, t_0) to (x, t) within the rarefaction wave, then the slope would be (Sod, 1978; Toro, 2009)

$$\frac{dx}{dt} = \frac{x}{t} = u - a\,, \tag{4.55}$$

where u is the fluid velocity and a sound speed

$$a = \sqrt{\gamma\frac{p}{\rho}}\,. \tag{4.56}$$

Sod (1978); Toro (2009); Zel'dovich and Raizer (1966) state, that the Riemann invariant is constant and therefor

$$u_1 + \frac{2\,a_1}{\gamma-1} = u_2 + \frac{2\,a_2}{\gamma-1}\,. \tag{4.57}$$

The isentropic law (Sod, 1978; Toro, 2009) gives an relation between the pressure and the density of the fluid

$$p = C\,\rho^{\gamma}\,. \tag{4.58}$$

The constant C can be evaluated through the initial conditions (Toro, 2009) and, therefor, resulting in

$$p_2 = p_1 \left(\frac{\rho_2}{\rho_1}\right)^{\gamma} . \tag{4.59}$$

By solving the equations 4.55, 4.56, 4.57 and 4.59 simultaneously, one finds the solution for the density, pressure and velocity within the rarefaction wave.

Solve for the velocity u_2:
Equation 4.55 can be rearranged to the velocity u_2,

$$u_2 = \frac{x}{t} + a_2 . \tag{4.60}$$

Equation 4.56 can be rearranged to the sound speed a_2,

$$a_2 = \frac{\gamma - 1}{2} \left[u_1 + \frac{2\, a_1}{\gamma - 1} - u_2 \right] \tag{4.61}$$

and replacing a_2 in Eq. 4.60 gives

$$u_2 = \frac{x}{t} + \frac{\gamma - 1}{2} \left[u_1 + \frac{2\, a_1}{\gamma - 1} - u_2 \right] . \tag{4.62}$$

By multiplying out the brace and collecting all terms with u_2 on the left side, one gets

$$u_2 \left(1 + \frac{\gamma - 1}{2} \right) = \frac{x}{t} + \frac{\gamma - 1}{2} u_1 + a_1 . \tag{4.63}$$

Isolating u_2 on the left side and using

$$1 + \frac{\gamma - 1}{2} = \frac{\gamma + 1}{2} \tag{4.64}$$

the final expression for the velocity is

$$u_2 = \frac{2}{\gamma + 1} \left[\frac{x}{t} + \frac{\gamma - 1}{2} u_1 + a_1 \right] . \tag{4.65}$$

Solve for the density ρ_2:
By inserting Eq. 4.60 in Eq. 4.57 one gets

$$u_1 + \frac{2\,a_1}{\gamma - 1} = \frac{x}{t} + a_2 + \frac{2\,a_2}{\gamma - 1} \tag{4.66}$$

$$= \frac{x}{t} + a_2 \left(1 + \frac{2}{\gamma - 1}\right) . \tag{4.67}$$

By using

$$1 + \frac{2}{\gamma - 1} = \frac{\gamma + 1}{\gamma - 1} \tag{4.68}$$

and rearranging to a_2 results in

$$a_2 = \frac{\gamma - 1}{\gamma + 1} u_1 + \frac{2\,a_1}{\gamma + 1} - \frac{\gamma - 1}{\gamma + 1} \frac{x}{t} \tag{4.69}$$

$$= \frac{2\,a_1}{\gamma + 1} + \frac{\gamma - 1}{\gamma + 1} \left(u_1 - \frac{x}{t}\right) . \tag{4.70}$$

Now one evaluates the sound speed by inserting Eq. 4.59 in Eq. 4.56:

$$a_2 = \left(\gamma \frac{p_2}{\rho_2}\right)^{\frac{1}{2}} \tag{4.71}$$

$$= \left(\gamma \frac{p_1}{\rho_1^\gamma} \frac{\rho_2^\gamma}{\rho_2}\right)^{\frac{1}{2}} . \tag{4.72}$$

Using the algebraic manipulation

$$\frac{\rho_2^\gamma}{\rho_2} = \rho_2^{\gamma - 1} \tag{4.73}$$

$$\rho_1^\gamma = \rho_1 \rho_1^{\gamma - 1} \tag{4.74}$$

one gets

$$a_2 = \left[\gamma \frac{p_1}{\rho_1} \left(\frac{\rho_2}{\rho_1}\right)^{\gamma - 1}\right]^{\frac{1}{2}} \tag{4.75}$$

$$= \sqrt{\gamma \frac{p_1}{\rho_1}} \left(\frac{\rho_2}{\rho_1}\right)^{\frac{\gamma - 1}{2}} \tag{4.76}$$

$$= a_1 \left(\frac{\rho_2}{\rho_1}\right)^{\frac{\gamma - 1}{2}} \tag{4.77}$$

Inserting Eq. 4.77 in Eq. 4.70

$$a_1 \left(\frac{\rho_2}{\rho_1}\right)^{\frac{\gamma-1}{2}} = \frac{2\,a_1}{\gamma+1} + \frac{\gamma-1}{\gamma+1}\left(u_1 - \frac{x}{t}\right) \quad | : a_1 \tag{4.78}$$

$$\left(\frac{\rho_2}{\rho_1}\right)^{\frac{\gamma-1}{2}} = \frac{2}{\gamma+1} + \frac{\gamma-1}{(\gamma+1)\,a_1}\left(u_1 - \frac{x}{t}\right). \tag{4.79}$$

Rearranging to ρ_2 on the left side gives the final expression for the density

$$\rho_2 = \rho_1 \left[\frac{2}{\gamma+1} + \frac{\gamma-1}{(\gamma+1)\,a_1}\left(u_1 - \frac{x}{t}\right)\right]^{\frac{2}{\gamma-1}}. \tag{4.80}$$

Solve for the pressure p_2:
Rearranging Eq. 4.59 to a ratio between pressures and densities:

$$p_2 = \frac{p_1}{\rho_1^{\gamma}}\rho_2^{\gamma} \quad \Leftrightarrow \quad \left(\frac{p_2}{p_1}\right)^{\frac{1}{\gamma}} = \frac{\rho_2}{\rho_1} \tag{4.81}$$

and using

$$\left(\frac{\rho_2}{\rho_1}\right)^{\frac{\gamma-1}{2}} = \left[\left(\frac{p_2}{p_1}\right)^{\frac{1}{\gamma}}\right]^{\frac{\gamma-1}{2}} = \left(\frac{p_2}{p_1}\right)^{\frac{\gamma-1}{2\gamma}} \tag{4.82}$$

gives

$$\left(\frac{p_2}{p_1}\right)^{\frac{\gamma-1}{2\gamma}} = \frac{2}{\gamma+1} + \frac{\gamma-1}{(\gamma+1)\,a_1}\left(u_1 - \frac{x}{t}\right) \tag{4.83}$$

Isolating p_2 on the left side gives the final expression for the pressure:

$$p_2 = p_1 \left[\frac{2}{\gamma+1} + \frac{\gamma-1}{(\gamma+1)\,a_1}\left(u_1 - \frac{x}{t}\right)\right]^{\frac{2\gamma}{\gamma-1}}. \tag{4.84}$$

To take into account that the initial position of the diaphragm at $t = 0$ is at $d > 0$, the

equations 4.65, 4.80 and 4.84 have to be modified to

$$u_2 = \frac{2}{\gamma+1}\left[\frac{(x-d)}{t} + \frac{\gamma-1}{2}u_1 + a_1\right] \tag{4.85}$$

$$\rho_2 = \rho_1\left[\frac{2}{\gamma+1} + \frac{\gamma-1}{(\gamma+1)\,a_1}\left(u_1 - \frac{(x-d)}{t}\right)\right]^{\frac{2}{\gamma-1}} \tag{4.86}$$

$$p_2 = p_1\left[\frac{2}{\gamma+1} + \frac{\gamma-1}{(\gamma+1)\,a_1}\left(u_1 - \frac{(x-d)}{t}\right)\right]^{\frac{2\gamma}{\gamma-1}} . \tag{4.87}$$

Position of the head and foot of the rarefaction wave:
To calculate the position of the head and foot of the rarefaction wave, the Eq. 4.55 is used, and modified to a form where the initial position of the diaphragm is not at zero. Region `II` is on the left side enclosed by region `I`, in that the head of the rarefaction wave is moving, therefor

$$xhd(t) = d + (u_1 - a_1)\,t\,, \quad t > 0\,. \tag{4.88}$$

The same can be done for the foot, where region `II` is on the right side enclosed by region `III`, in that the foot of the rarefaction wave is moving, therefor

$$xft(t) = d + (u_3 - a_3)\,t\,, \quad t > 0\,. \tag{4.89}$$

4.2.4 Region `III`

Sod (1978) states that the velocity and pressure are constant over a contact discontinuity, therefor:

$$u_3 = u_4 \tag{4.90}$$

$$p_3 = p_4 \tag{4.91}$$

Starting from the isentropic law (Eq. 4.59), an expression for the density can be obtained.

$$p_3 = p_4 = \frac{p_1}{\rho_1^\gamma}\rho_3^\gamma \tag{4.92}$$

Rearranging to ρ_3 gives

$$\rho_3 = \rho_1\left(\frac{p_4}{p_1}\right)^{\frac{1}{\gamma}} \tag{4.93}$$

The sound speed of a fluid in region III can also be expressed as a ration of the pressures. Using the definition of the sound speed (Eq. 4.56), and inserting the density (Eq. 4.93).

$$a_3 = \left(\gamma \frac{p_4}{\rho_3}\right)^{\frac{1}{2}} \tag{4.94}$$

$$= \left[\gamma \frac{p_4}{\rho_1} \left(\frac{p_1}{p_4}\right)^{\frac{1}{\gamma}}\right]^{\frac{1}{2}} \tag{4.95}$$

$$= \left[\gamma \frac{p_1^{\frac{1}{\gamma}}}{\rho_1} \frac{p_4}{p_4^{\frac{1}{\gamma}}}\right]^{\frac{1}{2}} \tag{4.96}$$

Using the algebraic manipulation

$$p_1^{\frac{1}{\gamma}} = p_1\, p_1^{\frac{1}{\gamma}-1} \tag{4.97}$$

$$\frac{p_4}{p_4^{\frac{1}{\gamma}}} = p_4^{1-\frac{1}{\gamma}}, \tag{4.98}$$

one gets

$$a_3 = \sqrt{\gamma \frac{p_1}{\rho_1}} \left(p_1^{\frac{1}{\gamma}-1}\, p_4^{1-\frac{1}{\gamma}}\right)^{\frac{1}{2}}. \tag{4.99}$$

Using the algebraic manipulation

$$\frac{1}{\gamma} - 1 = \frac{1-\gamma}{\gamma} = -\frac{\gamma-1}{\gamma} \tag{4.100}$$

$$1 - \frac{1}{\gamma} = \frac{\gamma-1}{\gamma}, \tag{4.101}$$

Eq. 4.99 transforms into

$$a_3 = a_1 \left[\left(\frac{p_4}{p_1}\right)^{\frac{\gamma-1}{\gamma}}\right]^{\frac{1}{2}} \tag{4.102}$$

$$= a_1 \left(\frac{p_4}{p_1}\right)^{\frac{\gamma-1}{2\gamma}}. \tag{4.103}$$

4.2.5 Region IV

To calculate the density, pressure and velocity behind the shock wave, one needs to find a relation between the states in region IV and the initial states. Following Toro (2009), one can evaluate the quantities $(\rho, p, u)_4$ on the left and right border of region IV.

Rarefaction Wave:
Starting on the left border of region `IV`, region `III`. Considering that the Riemann invariant is constant (Sod, 1978; Toro, 2009; Zel'dovich and Raizer, 1966), one gets a relation between the velocity in region `I` and `III`, and since the velocities on both sides of the contact discontinuity are equal (Sod, 1978), a relation between the states in in region `I` and `IV`.

$$u_1 + \frac{2\,a_1}{\gamma - 1} = u_4 + \frac{2\,a_3}{\gamma - 1} \tag{4.104}$$

Inserting Eq. 4.103 and solving for the velocity u_4.

$$u_4 = u_1 + \frac{2\,a_1}{\gamma - 1} - \frac{2\,a_1}{\gamma - 1}\left(\frac{p_4}{p_1}\right)^{\frac{\gamma-1}{2\gamma}} \tag{4.105}$$

$$= u_1 + \frac{2\,a_1}{\gamma - 1}\left[1 - \left(\frac{p_4}{p_1}\right)^{\frac{\gamma-1}{2\gamma}}\right] \tag{4.106}$$

$$= u_1 - \frac{2\,a_1}{\gamma - 1}\left[\left(\frac{p_4}{p_1}\right)^{\frac{\gamma-1}{2\gamma}} - 1\right], \quad \text{as given in Toro (2009).} \tag{4.107}$$

Shock Wave:
Now, starting on the right border of region `IV`, region `V`, separated by a shock wave. Using the relative velocities Eq. 4.4 and 4.5, and introducing the mass flux Q (Toro, 2009) through the Rankine-Hugoniot condition (Eq. 4.6).

$$Q_5 \equiv -\rho_4\,\hat{u}_4 = -\rho_5\,\hat{u}_5 \tag{4.108}$$

Now, rearranging Eq. 4.7 to

$$(\rho_4\,\hat{u}_4)\,\hat{u}_4 + p_4 = (\rho_5\,\hat{u}_5)\,\hat{u}_5 + p_5 \tag{4.109}$$

and inserting the mass flux

$$-Q_5\hat{u}_4 + p_4 = -Q_5\hat{u}_5 + p_5\,. \tag{4.110}$$

Rearranging to an expression for the mass flux gives

$$Q_5 = \frac{p_4 - p_5}{\hat{u}_4 - \hat{u}_5} \tag{4.111}$$

and re-substituting Eq. 4.4 and 4.5 gives

$$Q_5 = \frac{p_4 - p_5}{u_4 - u_5}\,. \tag{4.112}$$

From the mass flux one gets the relative velocities

$$\hat{u}_4 = -\frac{Q_5}{\rho_4} \tag{4.113}$$

$$\hat{u}_5 = -\frac{Q_5}{\rho_5} \tag{4.114}$$

and inserting them in Eq. 4.111 gives

$$Q_5 = \frac{p_4 - p_5}{Q_5\left(\frac{1}{\rho_5} - \frac{1}{\rho_4}\right)} \tag{4.115}$$

$$\Leftrightarrow \quad Q_5^2 = \frac{p_4 - p_5}{\frac{1}{\rho_5} - \frac{1}{\rho_4}}\,. \tag{4.116}$$

Inserting the relation 4.48 (Toro, 2009) gives the expression for the mass flux

$$Q_5 = \left[\frac{\rho_5}{2}\left(\frac{\gamma+1}{\gamma-1}\frac{p_4}{p_5} + 1\right)\right]^{\frac{1}{2}}\,. \tag{4.117}$$

By rearranging Eq. 4.112 to the velocity u_4 and inserting the new expression for the mass flux gives

$$u_4 = u_5 + \frac{p_4 - p_5}{Q_5} \tag{4.118}$$

$$= u_5 + (p_4 - p_5)\left[\frac{2}{\rho_5\left(\frac{\gamma+1}{\gamma-1}\frac{p_4}{p_5} + 1\right)}\right]^{\frac{1}{2}}\,. \tag{4.119}$$

Now, one has an expression for the velocity u_4 behind the shock front as a function of the initial states $(\rho_1, p_1, \rho_5, p_5)$ (Toro, 2009).

$$f(p_4) = \text{Eq. 4.107} - \text{Eq. 4.119} \tag{4.120}$$

$$= f_1(p_4, \rho_1, p_1) + f_5(p_4, \rho_5, p_5) + \Delta u \tag{4.121}$$

$$= \underbrace{\frac{2\,a_1}{\gamma - 1}\left[\left(\frac{p_4}{p_1}\right)^{\frac{\gamma-1}{2\gamma}} - 1\right]}_{f_1(p_4,\rho_1,p_1)} + \underbrace{(p_4 - p_5)\left[\frac{2}{\rho_5\left(\frac{\gamma+1}{\gamma-1}\frac{p_4}{p_5} + 1\right)}\right]^{\frac{1}{2}}}_{f_5(p_4,\rho_5,p_5)} + \underbrace{u_5 - u_4}_{\Delta u} \tag{4.122}$$

$$= 0 \tag{4.123}$$

This equation can be solved numerically for the pressure p_4 behind the shock front with a root finding method, such a the bisection method or the Newton-Raphson method. The actual velocity behind the shock front is the mean of the two velocities given by Eq. 4.107 and 4.119.

$$u_4 = \frac{1}{2}\big(u_5 + f_5(p_4, \rho_5, p_5)\big) + \frac{1}{2}\big(u_1 - f_1(p_4, \rho_1, p_1)\big) \tag{4.124}$$

$$= \frac{1}{2}\big(u_1 + u_5\big) + \frac{1}{2}\big[f_5(p_4, \rho_5, p_5) - f_1(p_4, \rho_1, p_1)\big] \tag{4.125}$$

The final density ρ_4 behind the shock front can be evaluated by Eq. 4.48.

Position of the contact discontinuity

Since the contact discontinuity separates region `III` from region `IV` and the velocity is the same in both regions (Sod, 1978), its position can be calculated as follows.

$$xcd(t) = d + u_4\,t\,, \qquad t > 0 \tag{4.126}$$

4.3 Complete Solution

This section gives an overview of the complete solution for the density ρ, pressure p and velocity u for each region, as well as the positions of the head and foot of the rarefaction wave, of the contact discontinuity and the shock front. Figure 4.3 displays the analytic solution for the density, pressure, velocity and internal energy of a fluid.

Solution: Region `I`

$$\rho_1 = 1.0 \quad | \quad p_1 = 1.0 \quad | \quad u_1 = 0.0 \tag{4.127}$$

Solution: Region `II`

$$\rho_2 = \rho_1 \left[\frac{2}{\gamma+1} \frac{\gamma-1}{(\gamma+1)\, a_1} \left(u_1 - \frac{x-d}{t} \right) \right]^{\frac{2}{\gamma-1}} \tag{4.128}$$

$$p_2 = p_1 \left[\frac{2}{\gamma+1} \frac{\gamma-1}{(\gamma+1)\, a_1} \left(u_1 - \frac{x-d}{t} \right) \right]^{\frac{2\gamma}{\gamma-1}} \tag{4.129}$$

$$u_2 = \frac{2}{\gamma+1} \left(a_1 + \frac{\gamma-1}{2} u_1 + \frac{x-d}{t} \right) \tag{4.130}$$

Solution: Region `III`

$$\rho_3 = \rho_1 \left(\frac{p_4}{p_1} \right)^{\frac{1}{\gamma}} \quad | \quad p_3 = p_4 \quad | \quad u_3 = u_4 \tag{4.131}$$

Solution: Region `IV`

$$\rho_4 = \rho_5 \left[\frac{p_4}{p_5} + \frac{\gamma-1}{\gamma+1} \right] \left[\frac{\gamma-1}{\gamma+1} \frac{p_4}{p_5} + 1 \right]^{-1} \tag{4.132}$$

$$p_4 \,:\, f(p_4) = \underbrace{\frac{2\, a_1}{\gamma-1} \left[\left(\frac{p_4}{p_1} \right)^{\frac{\gamma-1}{2\gamma}} - 1 \right]}_{f_1(p_4, \rho_1, p_1)} + \underbrace{(p_4 - p_5) \left[\frac{2}{\rho_5 \left(\frac{\gamma+1}{\gamma-1} \frac{p_4}{p_5} + 1 \right)} \right]^{\frac{1}{2}}}_{f_5(p_4, \rho_5, p_5)} + \underbrace{u_5 - u_4}_{\Delta u} = 0 \tag{4.133}$$

$$u_4 = \frac{1}{2} (u_1 + u_5) + \frac{1}{2} \left[f_5(p_4, \rho_5, p_5) - f_1(p_4, \rho_1, p_1) \right] \tag{4.134}$$

Solution: Region V

$$\rho_5 = 0.125 \quad | \quad p_5 = 0.1 \quad | \quad u_5 = 0.0 \tag{4.135}$$

Positions:

$$xhd(t) = d + (u_1 - a_1)\, t \tag{4.136}$$
$$xft(t) = d + (u_3 - a_3)\, t \tag{4.137}$$
$$xcd(t) = d + u_3\, t \tag{4.138}$$
$$xsh(t) = d + u_{sh}\, t\,, \qquad t > 0 \tag{4.139}$$

Toro (2009) provides results for the solution of the density pressure and velocity in region IV (Toro, 2009, table 4.1 and 4.3, Test 1). Table 4.1 gives a comparison of the solutions by Toro (2009) and by this work. The solutions for region II will not be compared, since it is not only time dependant but also depending on the position. As one can see, the derivation of the solution by this work agrees with those by Toro (2009).

Table 4.1: Comparison of the solution for the density ρ, pressure p and velocity u for the region IV by this work and Toro (2009). For this comparison, the same initial conditions (Eq. 4.1) are used and an adiabatic index of $\gamma = \frac{7}{5}$. The evaluation time is set to $t = 0.2\,\mathrm{s}$.

variable	*unit*	*analytic solution*	Toro (2009)
ρ_4	$[\mathrm{g\,cm^{-3}}]$	0.2655737	0.26557
p_4	$[\mathrm{dyne\,cm^{-2}}]$	0.3031301	0.30313
u_4	$[\mathrm{cm\,s^{-1}}]$	0.9274526	0.92745

Table 4.2 gives the positions of the head and foot of the rarefaction wave, the contact discontinuity and the shock front at a simulation time of $t = 0.2\,\mathrm{s}$. The shock wave has a speed of $u_{sh} = 1.75215\,\mathrm{cm\,s^{-1}}$.

Table 4.2: Position of the head and foot of the rarefaction wave, the contact discontinuity and the shock front at a simulation time of $t = 0.2\,\mathrm{s}$.

xhd [cm]	xft [cm]	xcd [cm]	xsh [cm]
0.26335	0.48594	0.68549	0.85943

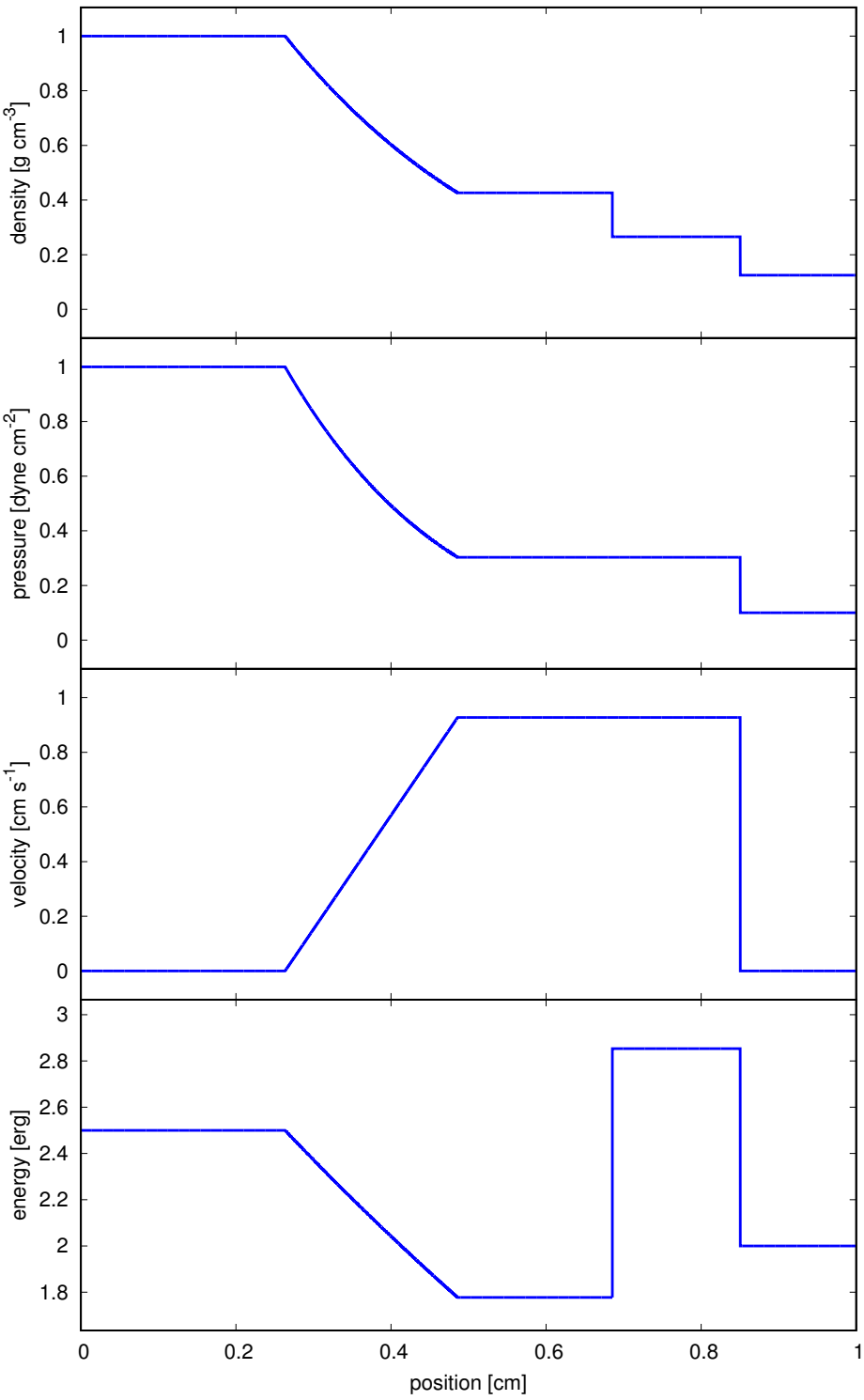

Figure 4.3: Analytic solution of the fluid density, pressure, velocity and internal energy at the time $t = 0.2\,\mathrm{s}$.

Chapter 5

Results

This chapter analyzes the results of the numerical simulation for the Sod Shock Tube Problem. Table 5.1 gives an overview of the various combinations of parameters for the different simulations that are performed. The simulation 4 (*sim4_ref*) is chosen to be the reference simulation for further comparisons.

Table 5.1: List of simulations with the following parameters: simulation ID *simID*, Courant number *CFL*, number of cells n_{cells}. The suffix "_ref" denotes to the reference simulation for the further comparisons.

simID	*CFL*	n_{cells}
sim1	0.2	100
sim2	0.2	300
sim3	0.2	500
sim4_ref	0.2	1000
sim5	0.4	1000
sim6	0.6	1000
sim7	0.8	1000

5.1 Analytical vs. Numerical Solution

For the comparison of the analytical and numerical solutions, simulation *sim4_ref* will be used. Figure 5.1 - 5.4 shows the results of the density, pressure, velocity and internal energy for the comparison of the analytical and numerical solutions of sim4_ref for the Sod Shock

Tube Problem. As one can see, the positions of the head and tail of the rarefaction wave, the contact discontinuity and the shock wave are relatively well captured. To quantify the results, the relative error (bottom panels of Fig. 5.1 - 5.4), given by

$$e_{rel} = \frac{s_n - s_a}{s_a}\,, \tag{5.1}$$

is calculated, where s_n and s_a are the numerical and analytical solution, respectively.
Looking closer at the head of the rarefaction wave, one can see that the position is not well computed. It is lacking behind the analytical solution and dropping rapidly. The relative error amounts up to 10 %, for the density and pressure. While it is lower for the internal energy, only up to 5 %, the error is relatively large for the velocity up to 100 %. For the foot of the rarefaction wave, the relative errors are quite low, up to almost 5 %. There, the values of the density, pressure and internal energy are slightly above those of the analytical solution, whereas it is for the velocity the other way around. There the values are slightly below the analytical ones.
Comparing the results for the contact discontinuity, one can see, that the relative errors are much larger. For the density the relative error amounts to 20 % shortly before the contact discontinuity and almost 30 % right after it. In the case of the internal energy, the error is around 23 %. It also is visible that the contact discontinuity is smeared out over a larger computational domain. Strictly speaking, it is a continuous change in density an energy, and not a discontinuous change in these quantities.
On the other hand, the shock wave is captured quite well, compared to the contact discontinuity. It spreads over a much smaller computational domain, but the relative errors a quite large for the density and pressure with an error larger than 60 %. The error is smaller for the velocity and internal energy of around 20 %.
Interestingly, the numerical solution of the rarefaction wave for the internal energy exhibits a peculiar behaviour. The rarefaction wave looks not continuously, but step wise.

5.2 Dependency on the Resolution

For the comparisons between simulations of different number of computing cells, the simulations *sim1*, *sim2*, *sim3* and *sim4_ref* will be compared. Figure 5.5 shows the density, pressure, velocity and internal energy for different number of cells. It can be seen that the numerical solution gets closer to the analytical solution with increasing number of computational cells. Figure 5.6 shows the relative errors of the state variables for different numbers of cells. For better comparison Fig. 5.7 shows a closeup of the head (left panel) and the foot (right panel) of the rarefaction wave.
For the head of the rarefaction wave, one can see that with increasing number of cells, that

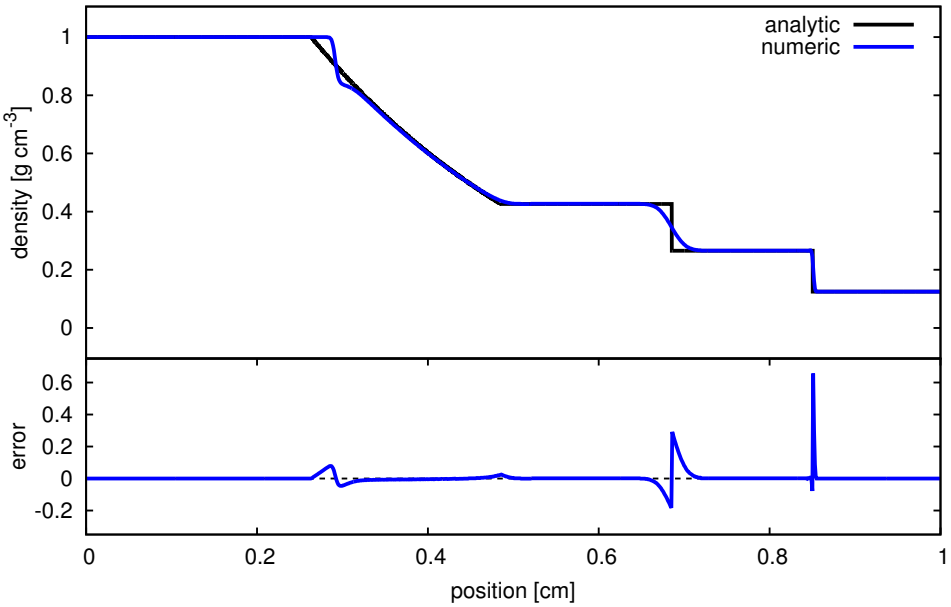

Figure 5.1: Top: Comparison of the results between the analytical (black) and numerical (blue) solution of the Sod shock problem for the density of a fluid at a simulation time of $t = 0.2\,\mathrm{s}$; Bottom: Relative error of the numerical solution in relation to the analytical solution.

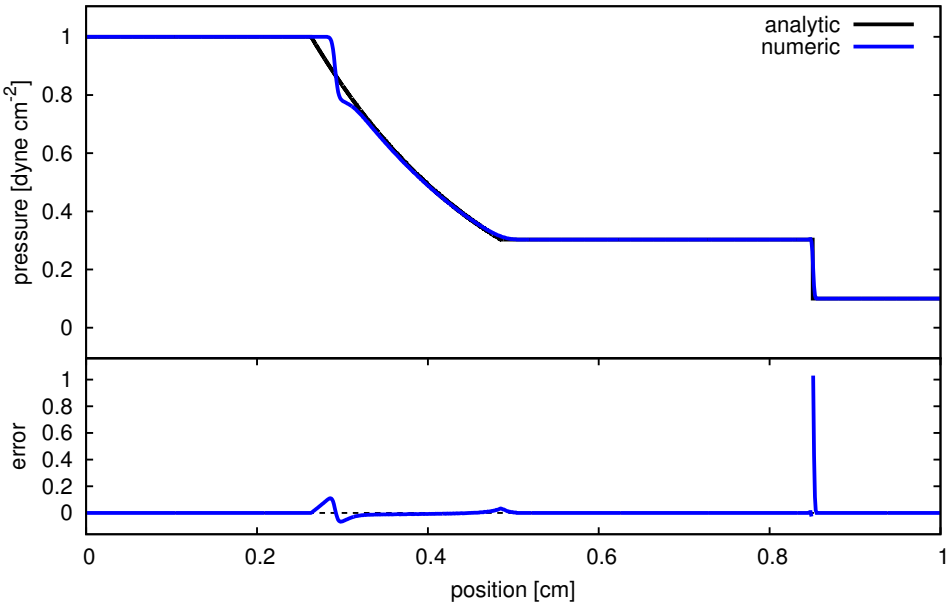

Figure 5.2: Same as figure 5.1 but for the pressure.

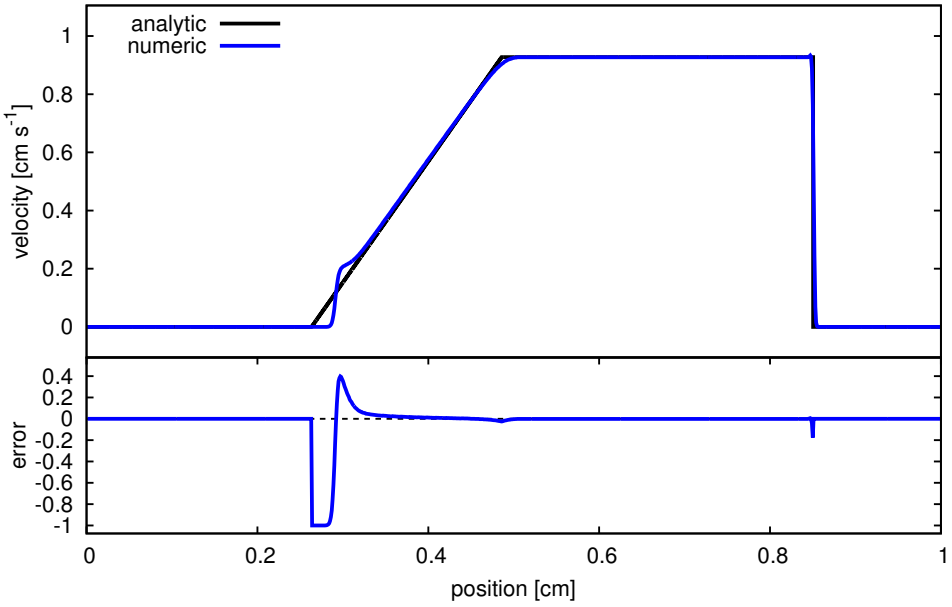

Figure 5.3: Same as figure 5.1 but for the velocity.

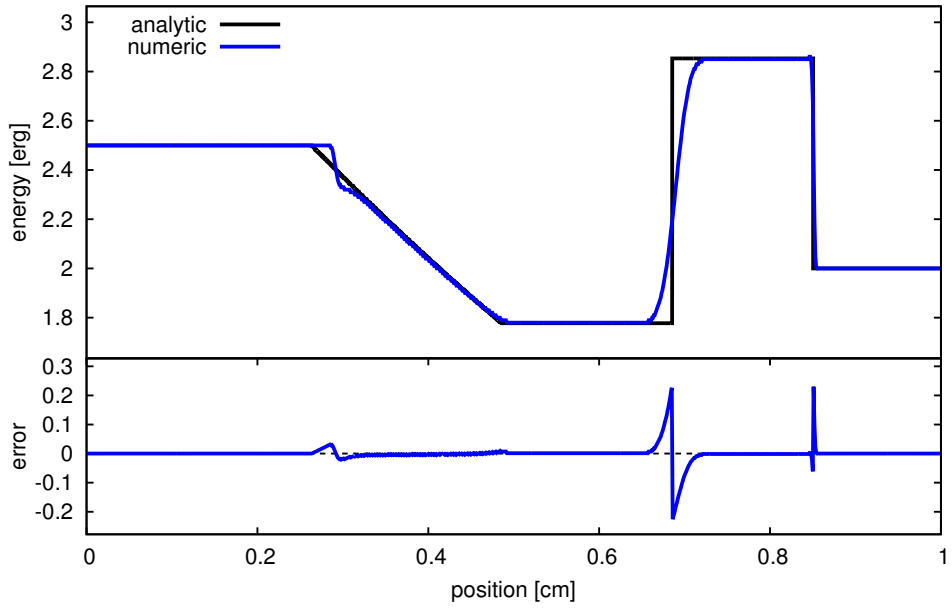

Figure 5.4: Same as figure 5.1 but for the internal energy.

another discontinuity is emerging. This can be seen for the density, pressure, velocity and energy. But also with increasing number of cells, the numerical solution gets closer to the analytical one.
For the foot of the rarefaction wave, the numerical solution gets closer to the analytical one with increasing number of cells. While the solution for the simulation *sim1* with only 100 cells clearly smears out the foot of the rarefaction wave and underestimates the density, pressure and energy (and overestimates the velocity), this quickly gets suppressed with increasing cell numbers.
Interestingly, the internal energy exhibits a stepwise numerical solution for the rarefaction wave. This gets more prominent with increasing number of computational cells.
Figure 5.8 shows a closeup of the shock wave of the density for different number of computational cells. The results for the pressure, velocity and internal energy look quite alike. It can clearly be seen, that for increasing number of cells the numerical solution gets closer to the analytical one. One can see, that the tipping point of the shock front gets closer to that of the analytical solution with increasing number of cells. Equally the thickness of the shock front is decreasing with increasing number of cells. Table 5.2 lists the position and the range of the shock front. Interestingly, the shock front is always resolved by five cells, although the thickness decreases with increasing number of cells. While the error for the solution of the density reaches quite large values right after the shock front, almost 65 % for the simulation *sim4_ref*, the error of the position of the shock front is decreasing with increasing resolution of the simulations. While the error is larger than 2 % for the run with the lowest resolution, it is smaller than 0.3 % for the run with the highest resolution.

Table 5.2: Position of the shock front $xsh(t)$, i.e. the 'head' and 'tail' of the shock wave, the number of cells $n_{cells,sh}$ over that the shock front is spread and the error of the position of the shock front for different models with their representative number of computational cells n_{cells} and the size of a single cell Δx at the simulation time $t = 0.2\,\mathrm{s}$.

model	n_{cells}	Δx	$xsh(t)$	$n_{cells,sh}$	*error*
analytic	–	–	0.8504	–	–
sim1	100	0.010	$0.8300 - 0.8900$	5	2.39%
sim2	300	0.003	$0.8433 - 0.8633$	5	0.84%
sim3	500	0.002	$0.8460 - 0.8580$	5	0.52%
sim4_ref	1000	0.001	$0.8480 - 0.8540$	5	0.28%

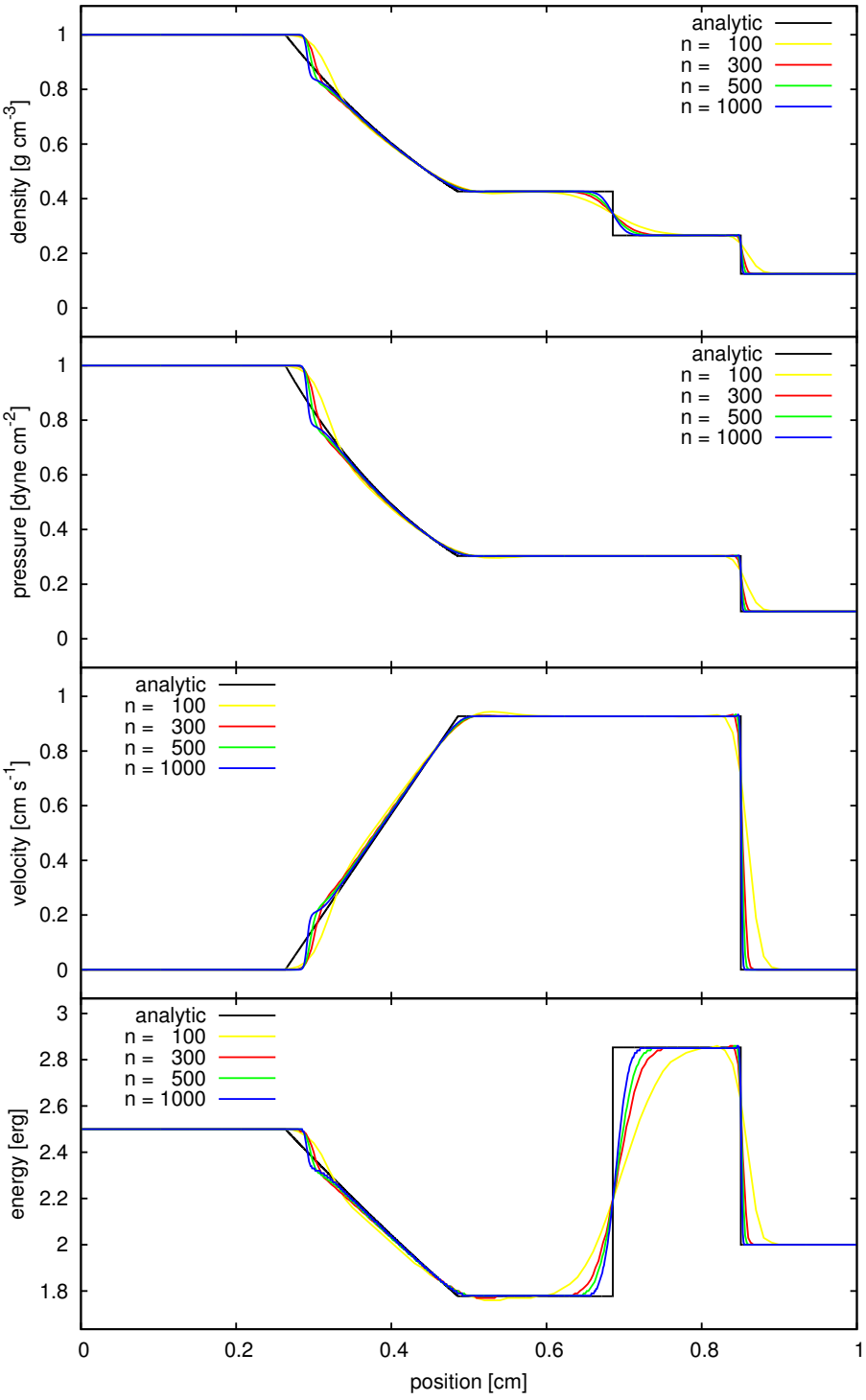

Figure 5.5: Comparison of the numerical solutions for different number of grid cells for the density, pressure, velocity and internal energy (from top to bottom) at the simulation time $t = 0.2\,\mathrm{s}$.

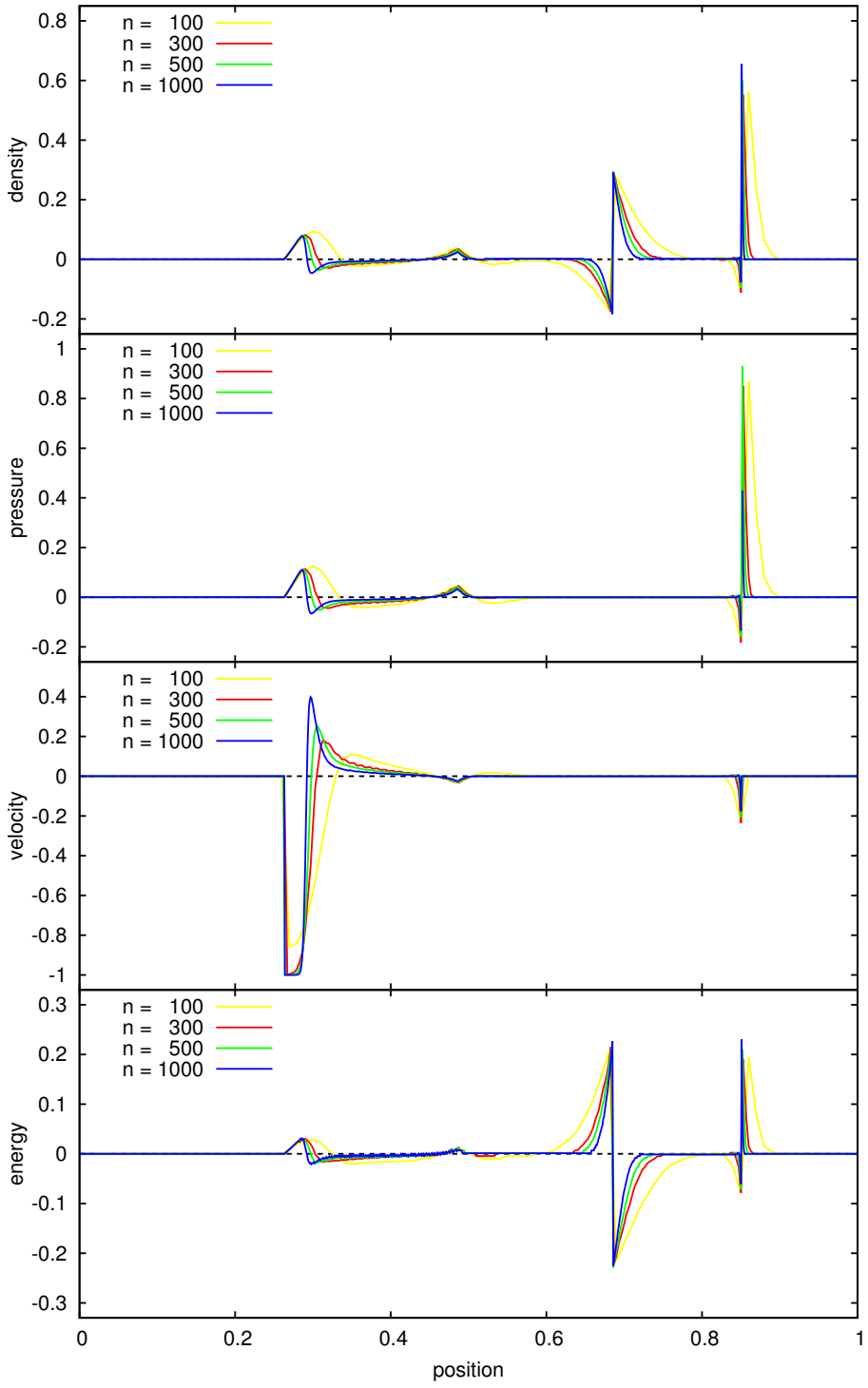

Figure 5.6: Comparison of the relative error of the numerical solutions for different number of grid cells for the density, pressure, velocity and internal energy (from top to bottom) at the simulation time $t = 0.2\,\mathrm{s}$.

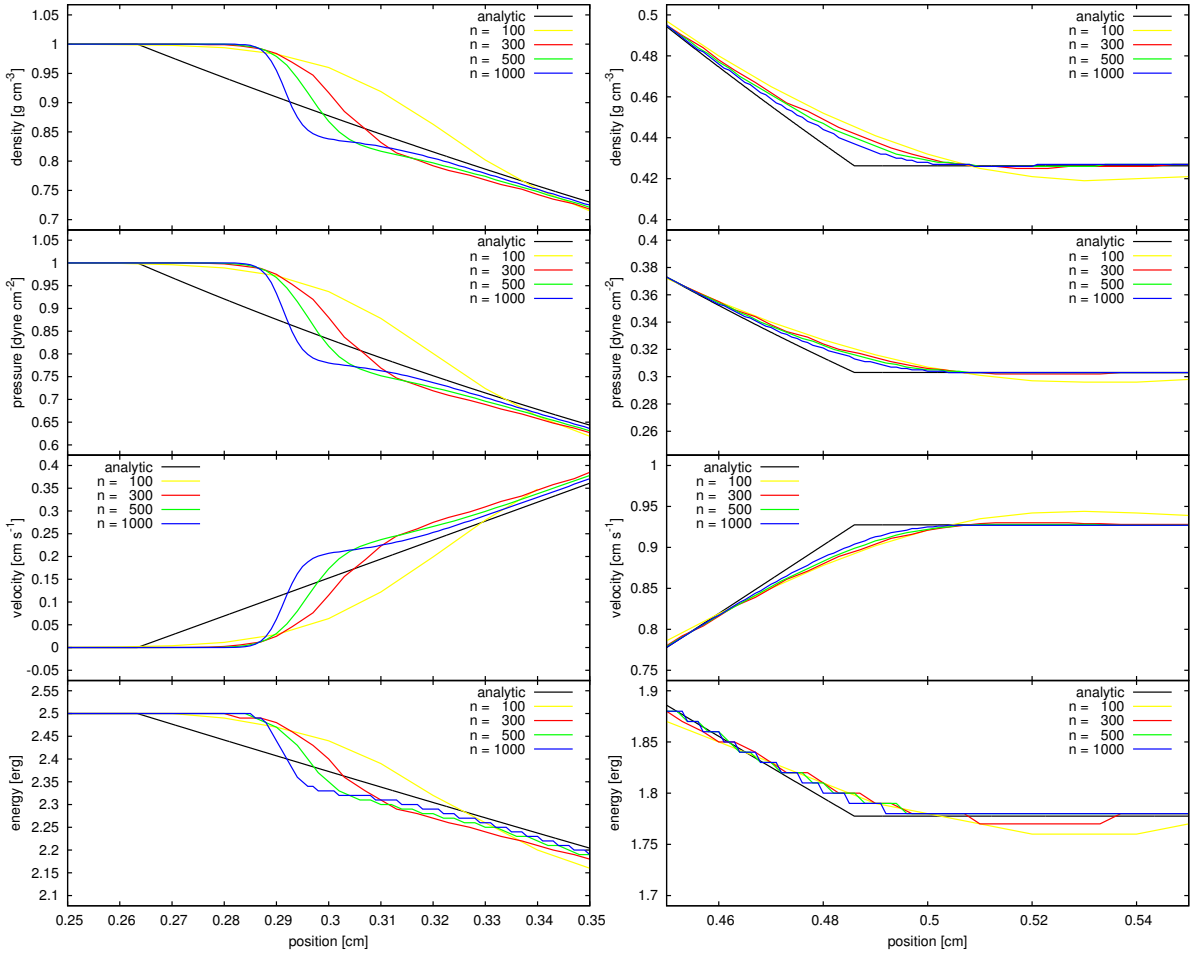

Figure 5.7: Zoom in on the head (left panel) and foot (right panel) of the rarefaction wave for a comparison of the numerical solutions for different number of grid cells for the density, pressure, velocity and internal energy (from top to bottom) at the simulation time $t = 0.2\,\mathrm{s}$.

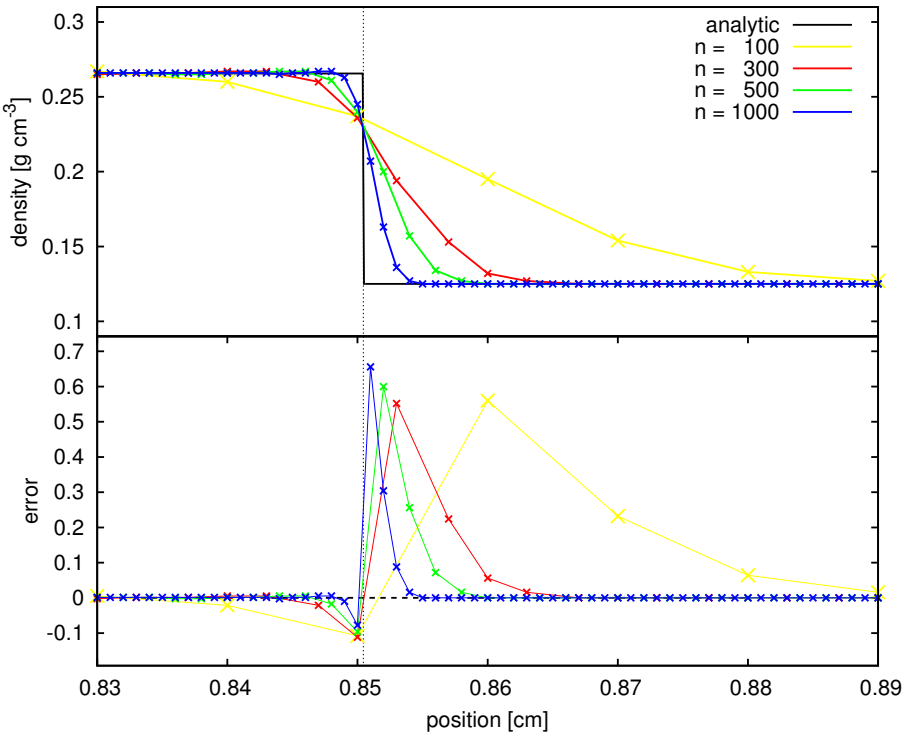

Figure 5.8: Zoom-in on the shock wave for a comparison of the numerical solutions for different number of grid cells for the density (top panel) and the relative errors (bottom panel) at the simulation time $t = 0.2\,\mathrm{s}$. The symbols (coloured crosses) represent the position of each cell. The vertical dotted line represents the position of the shock front and the horizontal dashed line (bottom panel) represents a relative error of zero.

5.3 Dependency on the CFL coefficient

For the comparison of the results for different CFL coefficients, the simulation *sim4_ref*, *sim5*, *sim6* and *sim7* are compared. Here, all simulations have the same number of computational cells of $n_{cell} = 1000$, but the CFL coefficient is varying, from 0.2 to 0.8.

Figure 5.9 shows the results for the density, pressure, velocity and internal energy for different values of the CFL coefficient and Fig. 5.10 its relative errors. As one can see, the results show two prominent effects with varying CFL coefficient. First, the formed discontinuity at the head of the rarefaction wave does not only get larger with increasing CFL coefficient, it also moves further away from the analytical solution. Second, the solution at the shock wave exhibits not only a peak, but an oscillation behind it which gets more prominent with increasing CFL coefficient.

Figure 5.11 shows a zoom-in of the shock front, where these oscillations are better visible. One can see, that the oscillations getting quickly damped with decreasing CFL coefficient. The solution of the run with a CFL coefficient of 0.8 exhibits right before the shock front a

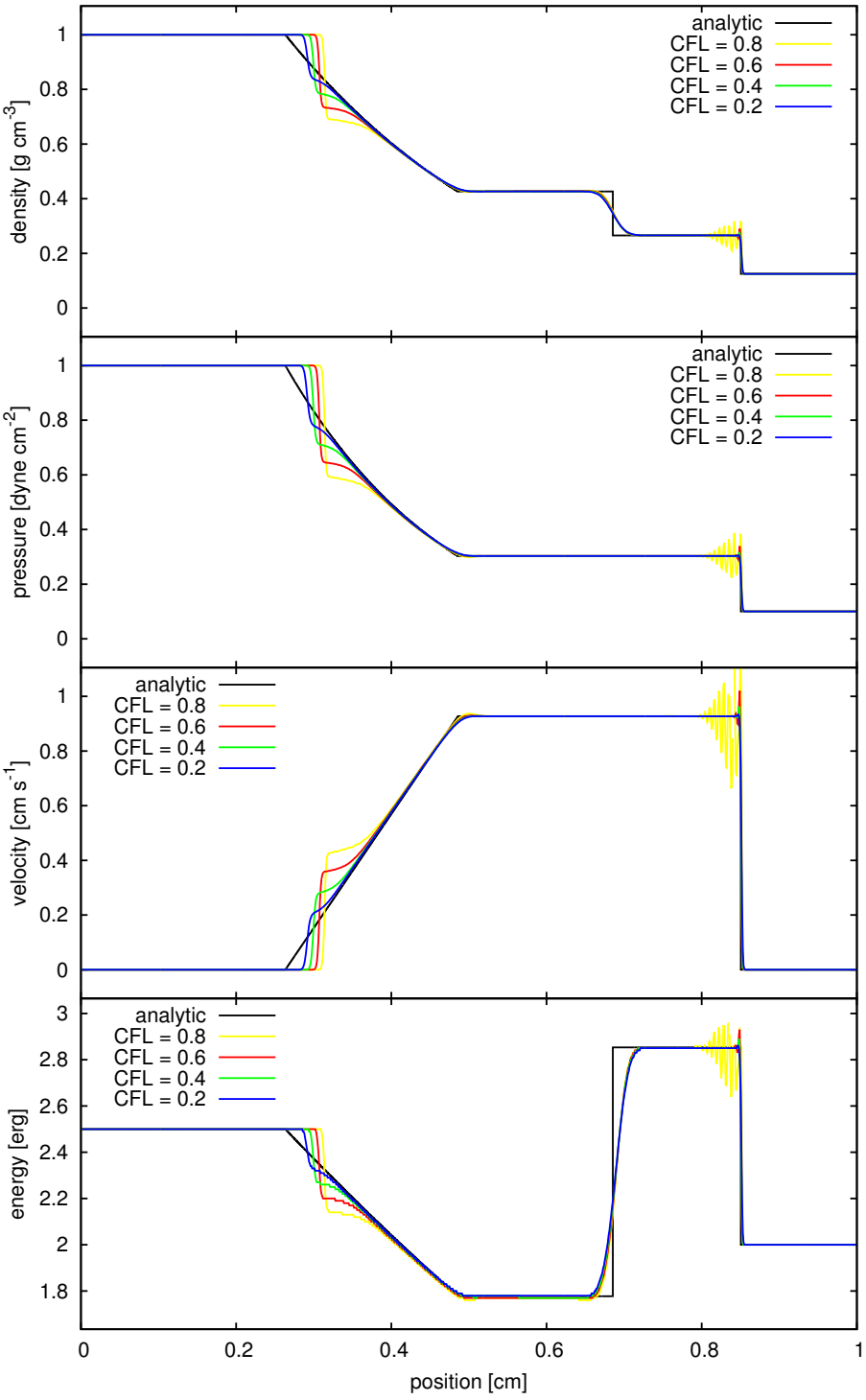

Figure 5.9: Comparison of the numerical solutions for different values of the CFL coefficient for the density, pressure, velocity and internal energy (from top to bottom) at the simulation time $t = 0.2\,\mathrm{s}$.

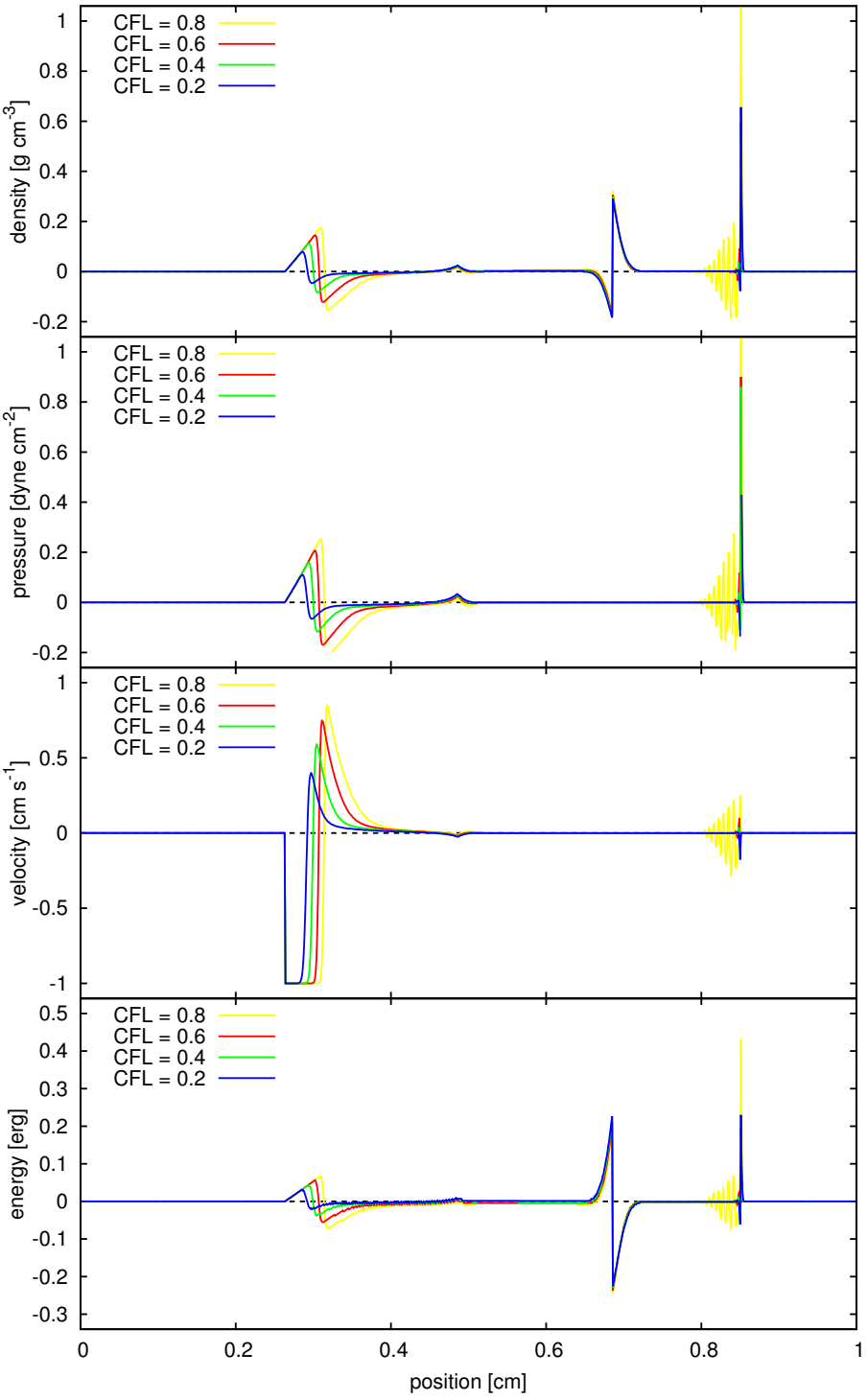

Figure 5.10: Comparison of the relative error of the numerical solutions for different values of the CFL coefficient for the density, pressure, velocity and internal energy (from top to bottom) at the simulation time $t = 0.2\,\mathrm{s}$.

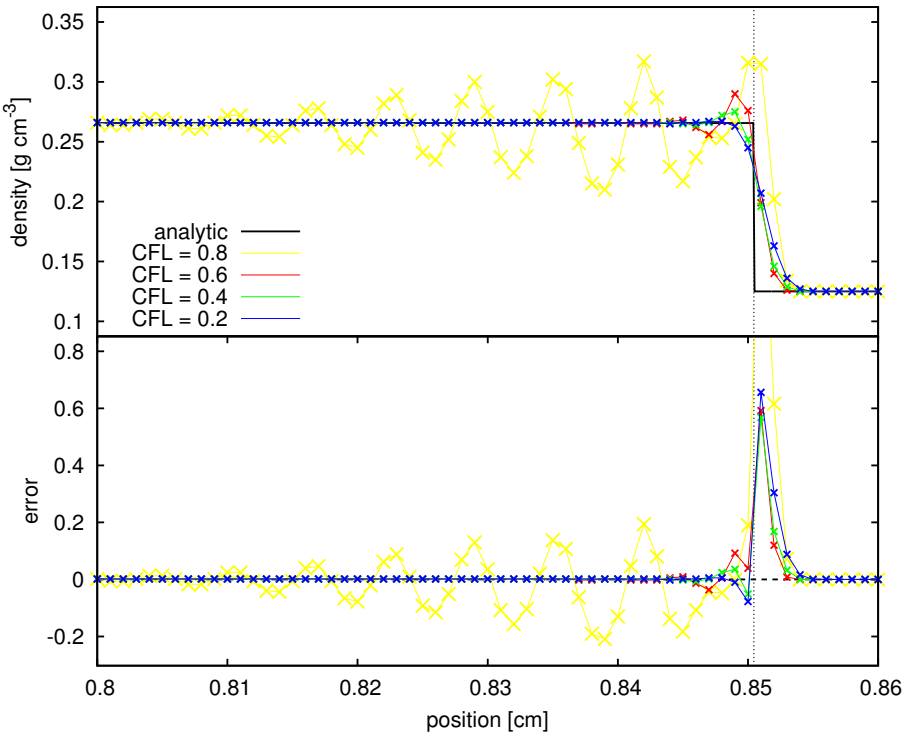

Figure 5.11: Zoom-in on the shock wave for a comparison of a different CFL coefficient for the density (top panel) and the relative errors (bottom panel) at the simulation time $t = 0.2\,\mathrm{s}$. The symbols (coloured crosses) represent the position of each cell. The vertical dotted line represents the position of the shock front and the horizontal dashed line (bottom panel) represents an relative error of zero.

quite large relative error of more than 150 %. This is due to the oscillation, which causes a peak at the shock front, which it is overshooting. This density peak (also counting for the other state variables) is resolved by two cells, where one cell is behind the shock front and the second one before, resulting in this large error.

Chapter 6

Discussion

This thesis presents an application of the "Sod Shock Tube Problem" to numerical studies by comparing the analytical solution with the numerical one. Therefore, a simple one-dimensional code is written to provide numerical data.

By comparing the solutions with different numbers of computational cells, one can quickly see that a larger number is desired for better results. The smaller the cell size, the smaller is the difference between two cells for a state variable. Therefore, by increasing the number of cells, thus decreasing the size of a computational cell, the results get more accurate and closer to the analytical solution. Mostly a small cell size is desired, which gets quickly computationally demanding, because it takes longer to loop over all cells. This can be avoided by using adaptive mesh refinement (AMR), which increases the resolution only there where the state variables are quickly changing. In case for the numerical description of the Sod Shock Tube Problem the resolution would only increase around the contact discontinuity, the shock front and along the rarefaction wave. One must emphasise that the higher resolution by AMR also depends on the level of refinement.
By comparing the solutions with different CFL coefficients, one can immediately see that a smaller CFL coefficient results in a more stable scheme. Durran (2010) states that a scheme with a CFL coefficient larger than one gets unstable. The comparison shows, that the scheme gets more unstable with increasing CFL coefficient, resulting with $C_{cfl} = 0.8$ in prominent oscillations behind the shock front. Furthermore, a larger CFL coefficient also causes a peak in the state variables at the position of the shock front. This can be prevented by implementing an artificial viscosity, which artificially damps emerging oscillations.
To overcome the short comes mentioned above, a better scheme can be used, that is second order accurate both in space and time. Nowadays, there are many sophisticated numerical codes. One example is the FLASH code (Fryxell et al., 2000; ASC FLASH Center, 2010). The FLASH code is a highly parallel code which uses the Massage-Passing Interface (MPI)

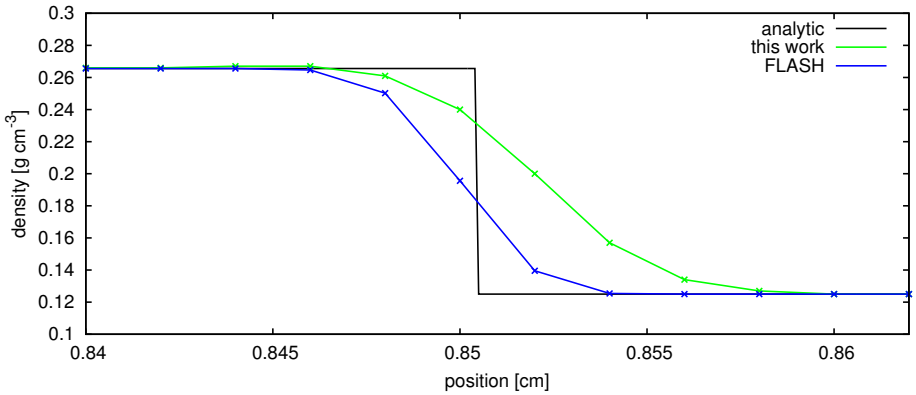

Figure 6.1: Comparison of the numerical solution of the run *sim3* with the FLASH code at the same resolution of $n_{cells} = 500$ and a simulation time of $t = 0.2\,\mathrm{s}$.

and AMR, and provides the user with several physical modules capable of dealing with hydrodynamics, self-gravity, thermal processes etc. Figure 6.1 shows a comparison between the analytical solutions of the run *sim3* and the FLASH code. For the simulation with the FLASH code, a uniform grid in 1D with an equal number of computational cells to the run *sim3* is used. Furthermore, the FLASH code uses the PPM (piecewise-parabolic method) hydro solver, where the flow variables are represented by piecewise-parabolic functions, which is second order accurate in space and time (ASC FLASH Center, 2010). As one can see, the position of the shock front calculated by the FLASH code is the same as those by the run *sim3* ($xsh(0.2\,\mathrm{s}) = 0.8460 - 0.8540$), but the shock wave is resolved by only three computational cells and much thinner.

Since shocks are quite common in nature, their treatment in numerical simulations must not be neglected. Sod (1978) provides a simple test to ensure that a numerical code can indeed resolve shocks. By adjusting basic parameters such as the number of computational cells or the Courrant-Friedrichs-Lewy condition one can improve the outcome. Advanced options like AMR and MPI can be used to minimise the computational effort and to maximise the efficiency.

Acknowledgements

I would like to thank my supervisor Maria Charina for her help and patience during my time on the diploma thesis.
The software used in this work was in part developed by the DOE NNSA-ASC OASCR Flash Center at the University of Chicago. The computational results presented have been achieved (in part) using the Vienna Scientific Cluster (VSC).

Abstract English

Nowadays, numerical simulations are widely used to investigate questions in physics in more detail. Most of these questions deal with the behaviour of fluids, such as gases and liquids. A quite interesting application for this is the field of astrophysics. Many phenomena in astrophysics are violent, for example the explosion of a star at the end of its lifetime as a supernova, where the surrounding material will be compressed. Such a compression results in a shock wave (*Stoßwelle* in german), which is propagating through the interstellar medium. Since shock waves are common in many applications, it is essential that numerical simulations are able to resolve and detect them. Because different kinds of codes use different numerical methods, they have to be tested in order to be certain that their solution is a acceptable. The "Sod Shock Tube Problem" is a method to test numerical codes, whether or not they can detect shock waves.

In this Diploma thesis the analytical and numerical solutions of the "Sod Shock Tube Problem" are compared. Therefore, first the analytical form of the continuous Euler equations is derived from major physical conservation principles. Further on, the change from the continuous to the discrete form of the Euler equations is explained, for that purpose the finite volume method is used. Based on this discrete description, a numerical code is written to simulate the "Sod Shock Tube Problem". The analytical solution of the corresponding problem will be derived in dependency on the initial conditions and compared graphically with the numerical solution. Furthermore, the dependency of the accuracy of the numerical code is investigated and discussed.

Abstract Deutsch

Heutzutage werden numerische Simulationen oft benutzt um bestimmte physikalische Fragestellungen genauer untersuchen zu können. Meistens beschäftigen sich solche Simulationen mit dem Verhalten von Gasen oder Flüssigkeiten. Ein sehr interessantes Anwendungsgebiet ist hierbei die Astrophysik. Viele Phänomene in der Astrophysik sind sehr energieintensiv, zum Beispiel die Explosion eines Sterns als Supernova, welche eine Verdichtung des umliegenden Gases verursacht. Solch eine Verdichtung bildet typischerweise eine Stoßwelle (*shock wave* im englischen), welche sich weiter ausbreitet. Da Stoßwellen in vielen Bereichen vorkommen, ist es essentiell, dass numerische Simulationen diese auch auf feinen Skalen beschreiben und erkennen können. Da unterschiedliche Codes verschiedene numerische Verfahren benutzen, muss getestet werden ob dieser eine physikalisch akzeptable Lösung liefert. Das "Sod Shock Tube Problem" ist ein Testverfahren um numerische Codes zu testen, ob sie Stoßwellen erkennen und korrekt beschreiben können.
In dieser Diplomarbeit werden die analytische und numerische Lösungen miteinander verglichen. Hierfür wird zuerst die analytische Lösung der stetigen Euler-Gleichung aus den wichtigsten physikalischen Erhaltungsprinzipien hergeleitet. Weiters wird mit Hilfe des Finite-Volumen-Verfahrens der Übergang von der stetigen zur diskreten Beschreibung der Euler-Gleichung erklärt. Ausgehend von der diskreten Beschreibung der Euler-Gleichungen wird dann ein numerischer Code geschrieben, um das "Sod Shock Tube Problem" computergestützt numerisch zu berechnen. Die analytische Lösung dieses Problems wird dann in Abhängigkeit der Anfangsbedingungen hergeleitet und graphisch mit der numerischen Lösung verglichen. Des Weiteren wird die Abhängigkeit der Genauigkeit der numerischen Lösung untersucht und diskutiert.

Bibliography

ASC FLASH Center (2010). *FLASH User's Guide - Version 3.3*.

Bartsch, H. (2007). *Taschenbuch Mathematischer Formeln*, volume 21. Carl Hanser Verlag.

Ben-Dor, G., Igra, O., and Elperin, T. (2000). *Handbook of Shock Waves, Three Volume Set*. Academic Press.

Christodoulou, D. and Miao, S. (2012). Compressible Flow and Euler's Equations. *ArXiv e-prints*.

Chung, S. M., Gonzalez, A. H., Clowe, D., Zaritsky, D., Markevitch, M., and Jones, C. (2009). Impacts of a Supersonic Shock Front on Star Formation in the Bullet Cluster. *APJ*, 691:963–970.

Durran, D. R. (2010). *Numerical Methods for Fluid Dynamics*. Springer, 2nd edition.

Ferziger, J. H. and Peric, M. (2002). *Computational Methods for Fluid Dynamics*. Springer, 3rd edition.

Fryxell, B., Olson, K., Ricker, P., Timmes, F. X., Zingale, M., Lamb, D. Q., MacNeice, P., Rosner, R., Truran, J. W., and Tufo, H. (2000). Flash: An adaptive mesh hydrodynamics code for modeling astrophysical thermonuclear flashes. *apjs*, 131(1):273–334.

Landau, L. D. and Lifshitz, E. M. (1987). *Fluid Mechanics*, volume 6 of Course of Theoretical Physics. Elsevier, 2nd edition.

Lequeux, J. (2010). *The Interstellar Medium*. Springer.

Raymond, J. C. (2018). Shock waves in interstellar gas and the solar corona. *Publications de l'Observatoire Astronomique de Beograd*, 98:59–68.

Rieutord, M. (2015). *Fluid Dynamics - An Introduction*. Springer.

Silber, E. A., Boslough, M., Hocking, W. K., Gritsevich, M., and Whitaker, R. W. (2018). Physics of meteor generated shock waves in the Earth's atmosphere - A review. *Advances in Space Research*, 62:489–532.

Sod, G. A. (1978). A survey of several finite difference methods for systems of nonlinear hyperbolic conservation laws. *Journal of Computational Physics*, 27:1–31.

Steyrleithner, P. (2015). Evolution of dwarf galaxies during the infall into galaxy clusters. Master's thesis, University of Vienna.

Toro, E. F. (2009). *Riemann Solvers and Numerical Methods for Flid Dynamic*. Springer, third edition.

Trangenstein, J. A. (2009). *Numerical Solutions Of Hyperbolic Partial Differential Equations*. Cambridgge.

Wikipedia contributors (2019). Chelyabinsk meteor — Wikipedia, The Free Encyclopedia.

Yun, K., Pillepich, A., Zinger, E., Nelson, D., Donnari, M., Joshi, G., Rodriguez-Gomez, V., Genel, S., Weinberger, R., Vogelsberger, M., and Hernquist, L. (2019). Jellyfish galaxies with the IllustrisTNG simulations - I. Gas-stripping phenomena in the full cosmological context. *MNRAS*, 483:1042–1066.

Zajacek, M., Eckart, A., and Elaheh Hosseini, S. (2019). Bow shock sources close to the Galactic centre. *arXiv e-prints*.

Zel'dovich, Y. B. and Raizer, Y. P. (1966). *Physics of Shock Waves and High-Temperature Hydrodynamic Phenomena*, volume I. Academic Press New York and London.